A functional map for diverse forelimb actions within brainstem circuitry

Ludwig Ruder1,2, Riccardo Schina1,2, Harsh Kanodia1,2, Sara Valencia-Garcia1,2, Chiara Pivetta1,2 & Silvia Arber1,2

1 Biozentrum, Department of Cell Biology, University of Basel, Basel, Switzerland.
2 Friedrich Miescher Institute for Biomedical Research, Basel, Switzerland.
Correspondence to: silvia.arber@unibas.ch

Nature **590,** 445–450 (2021)

The brainstem is a key centre in the control of body movements. Although the precise nature of brainstem cell types and circuits that are central to full-body locomotion are becoming known[1–5], efforts to understand the neuronal underpinnings of skilled forelimb movements have focused predominantly on supra-brainstem centres and the spinal cord[6–12]. Here we defne the logic of a functional map for skilled forelimb movements within the lateral rostral medulla (latRM) of the brainstem. Using in vivo electrophysiology in freely moving mice, we reveal a neuronal code with tuning of latRM populations to distinct forelimb actions. These include reaching and food handling, both of which are impaired by perturbation of excitatory latRM neurons. Through the combinatorial use of genetics and viral tracing, we demonstrate that excitatory latRM neurons segregate into distinct populations by axonal target, and act through the diferential recruitment of intra-brainstem and spinal circuits. Investigating the behavioural potential of projection-stratifed latRM populations, we find that the optogenetic stimulation of these populations can elicit diverse forelimb movements, with each behaviour stably expressed by individual mice. In summary, projection-stratifed brainstem populations encode action phases and together serve as putative building blocks for regulating key features of complex forelimb movements, identifying substrates of the brainstem for skilled forelimb behaviours.

Understanding how diverse body movements are regulated necessitates the identification of neuronal circuit mechanisms that are central to this process. The brainstem represents a key integration and processing junction that establishes links between upper motor centres involved in planning actions and circuits in the spinal cord that are required for execution of body movements[6,8,13–18]. Specific neuronal circuits within the brainstem and their outputs to the spinal cord are dedicated to the regulation of locomotion[1–5], a behaviour that requires full-body coordination. Whether neuronal circuit modules devoted specifically to skilled forelimb movements exist within the brainstem, and how they interact with spinal circuits and coordinate the construction of complex forelimb movements is poorly understood. A major historical focus in understanding how the nervous system regulates skilled forelimb movements has been on higher motor centres, including motor cortex and basal ganglia[6–10,19]. However, several lines of evidence suggest that the execution of skilled forelimb movements engages and is dependent on subcortical structures, especially the brainstem. Evolutionary analysis demonstrates that behavioural elements of skilled forelimb movements, including reaching and food handling, are already present in species without corticospinal tracts (including frogs)[20]. In mice, the ablation of specific excitatory neurons in the caudal medulla impairs food grasping[21]. The medulla and pons of the brainstem also contain neurons that are recruited during forelimb reaching in cats[22,23] and digit movements in monkeys[24]. Monkeys with lesions of the corticospinal tract compensate all aspects of skilled forelimb movements, except the use of single digits[25,26]. Notably, an additional specific lesion of the lateral—but not the medial—lower brainstem entirely abrogates these behavioural compensations[26,27]. Finally, systematic electrical microstimulation experiments in these regions, albeit focused on locomotion as read-out, have identified sites within the lateral medulla, the stimulation of which elicited specifically forelimb movements with no effects on hindlimbs[28]. Together, these findings point to the existence of important, yet uncharacterized, neuronal substrates in the lateral medulla that are required for the execution of skilled forelimb movements.

LatRM neurons tuned to forelimb actions

To assess the activity of neurons in the latRM, we performed in vivo recordings using chronic silicon probe implants in the mouse brainstem. We centred the implant in the parvicellular reticular nucleus[29] at the rostrocaudal level of the facial nucleus (Extended Data Fig. 1a, b), a region of the brainstem in which we had observed neurons specifically premotor to motor neurons innervating forelimb muscles[21]. This allowed us to monitor the activity of single neurons while freely moving mice performed different behavioural tasks (Fig. 1, Extended Data Fig. 1). We trained mice on a food-pellet reaching and retrieval task (hereafter, pellet task) to specifically engage in unilateral forelimb reaching and subsequent food handling[30]. As a distinct but behaviourally similar forelimb-engaging task, we trained mice to reach for and press a lever (hereafter, lever task), the successful execution of which allowed them to retrieve a reward[31]. To contrast these mostly forelimb-engaging behaviours, we assessed latRM neuron activity during full-body locomotion, which represents a behaviour that also strongly engages forelimb muscles but does so in a very different context. To get an overview of activity changes of latRM neurons during a task, we analysed the mean-subtracted firing rate of all neurons tuned to one of the two forelimb tasks. We observed a notable overall increase in firing rate during each of the forelimb tasks (pellet and lever tasks), but not during locomotion or when analysing shuffled data from the same neurons (Fig. 1a). For both forelimb tasks, individual neurons contributed to the overall curve by tiling the behavioural space from preparation to execution (Fig. 1a), and a large majority of neurons upregulated their firing rate (Extended Data Fig. 1c, d). Analysis of the changes in firing profile revealed diversity, with selectivity to particular time windows (Fig. 1a; Extended Data Fig. 1e–g). We next addressed the question of whether populations of latRM neurons are tuned to specific behavioural phases. We analysed changes in neuronal activity during sharp, behaviourally defined time windows (Methods). We identified neurons tuned to the reaching phase of the pellet or lever task (relatively similar forelimb actions), and compared these to neurons tuned to food

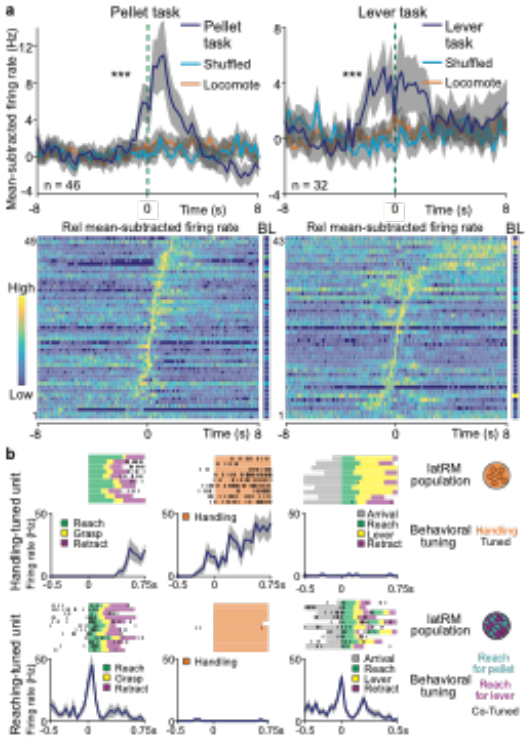

Fig. 1 | Brainstem neurons specifically tuned to forelimb behaviours. a, Mean subtracted firing rate of all task-tuned latRM neurons analysed for the pellet (left) and lever (right) tasks, depicting average over all neurons (top; recorded also in locomotion) or individual neurons sorted by time of maximal relative mean subtracted firing rate (bottom, recorded in shown task), with time 0 representing reaching onset. Bottom, colour scale shows low (0) to high (1) for relative mean-subtracted firing rate and low (0 Hz) to high (100 Hz) for baseline (BL) firing rate. Top, average of mean-subtracted firing rate of the task-tuned latRM neurons identified commonly in all tasks considered during onset of locomotion trials (locomote) or shuffled data. n = 5 mice; n = 46 neurons assessed during both pellet task and locomotion; n = 32 for neurons assessed during both lever task and locomotion (Methods). b, Examples for two latRM neurons during pellet task (left), food handling (middle) and lever task (right). Behavioural phases are marked in colour for all trials and summary schemes are shown on the right. Example unit on the top displays tuning preference for handling over other behavioural phases; the bottom unit displays tuning preference for reaching (for lever or pellet) over handling (average firing rate in Hz is shown below single trials; n = 1 example neuron each). Grey shade denotes ±s.e.m. ***P<0.00033; Wilcoxon signed-rank test. Bonferroni correction was applied to account for multiple comparisons.

Extended Data Fig. 1 | Methodological approaches and firing properties of latRM neurons. a, Scheme outlining experimental setup and analysis pipeline for single unit recordings of latRM neurons. A total of 194 neurons were recorded in lever task, pellet task and open field assay. b, Representative latRM section from mouse undergoing single-unit recordings, depicting end point of silicon probe trajectory, visualized through electrical lesion (arrow) performed at the end of all recording sessions, counterstained for ChAT to visualize 7N neurons. c, Analysis of average firing rates of behaviourally relevant neurons for pellet (left, n = 84 neurons) and lever (right, n = 81 neurons) tasks, demonstrating that most neurons fire at relatively low rates. d, Analysis of changes in firing rate of task-tuned neurons comparing baseline to behaviour. The large majority of neurons upregulate their firing rate, and only few downregulate it (n = 43 neurons for lever task, n = 49 neurons for pellet task). e, f, Two examples of raw unsorted traces (e), aligned to reaching (left) or handling (right) onset, depicting the spiking pattern of the subsequently sorted unit below with indication of behavioural time windows. Waveforms for these two units are shown for lever and pellet tasks, which were carried out sequentially. g, Recordings from seven example LatRM neurons during lever or pellet task, displaying single trials aligned to behavioural phases (spikes shown as lines) as well as average firing rate (Hz) below single trials (n = 1 neuron each); grey shade, ±s.e.m.

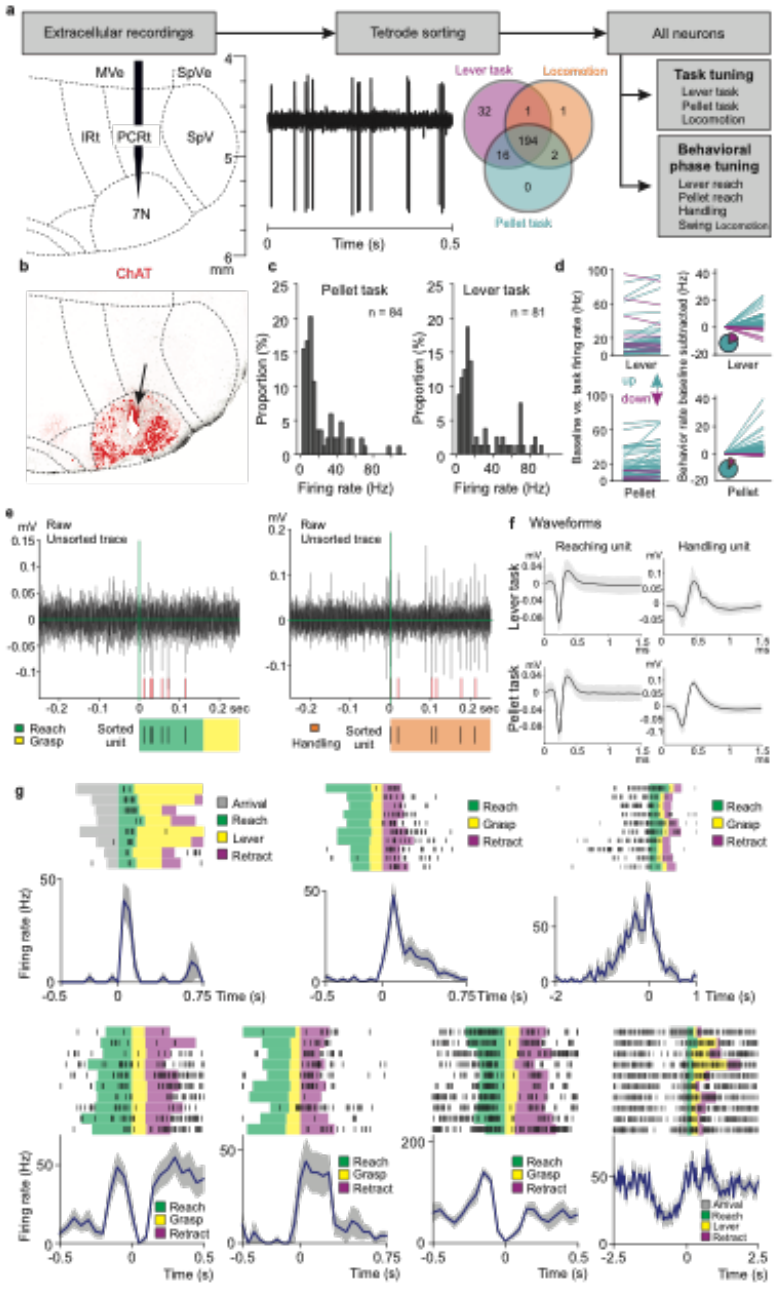

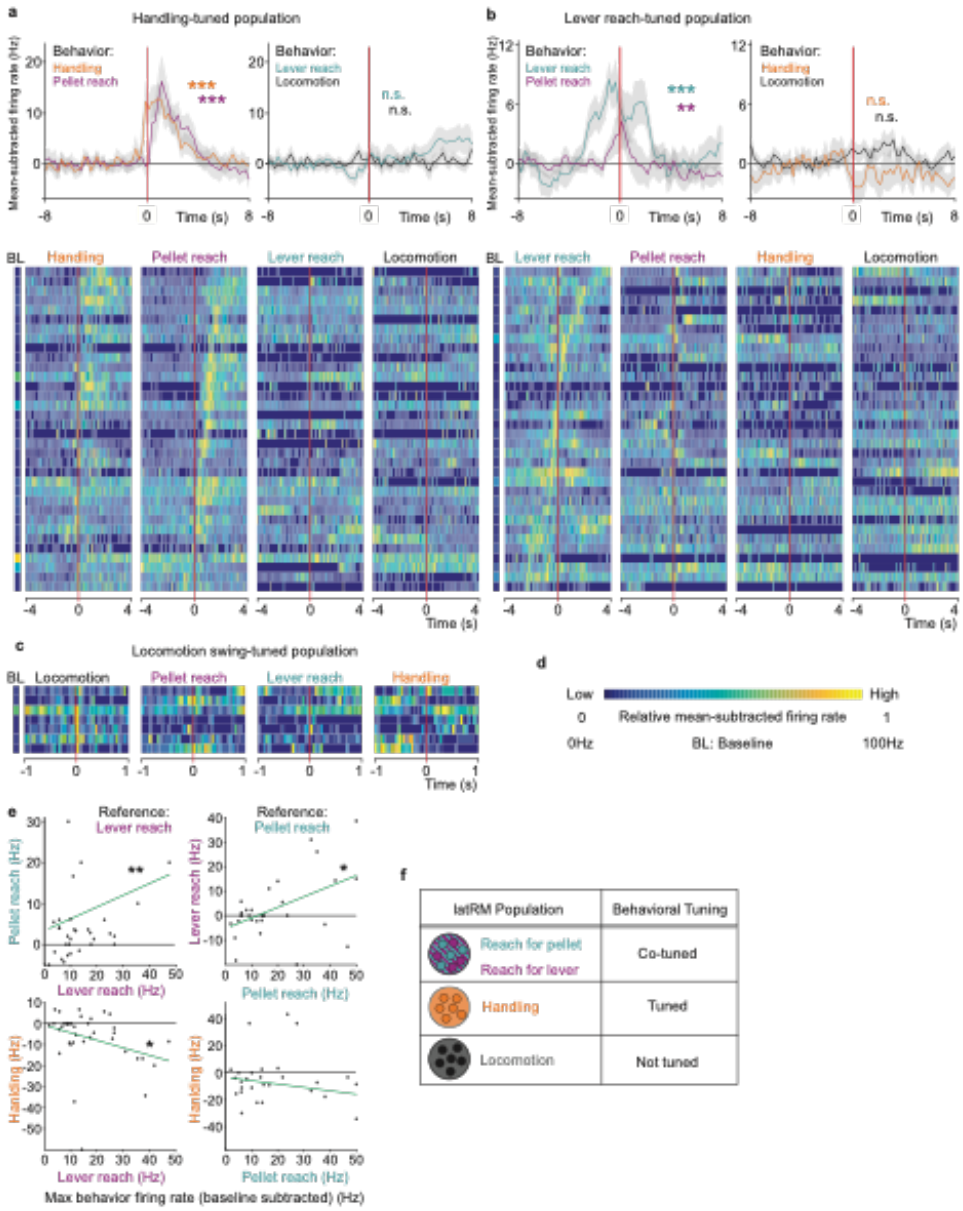

Extended Data Fig. 2 | Behavioural tuning properties of latRM neurons. a–d, Analysis of handling-tuned (a) and lever-reach-tuned (b) latRM populations (n = 34 neurons each), depicting response properties of all respective neurons aligned to behavioural onset of handling, pellet reach, lever reach or locomotion swing phase (top: average of all neurons, bottom: raster plot for individual neurons ordered by peak time of pellet reach) (a) or lever reach (b). c, Data depicted in raster plots for the small number of latRM neurons making up a locomotion swing-phased tuned latRM population. Colour scale in d depicts low (0) to high (1) for relative mean-subtracted firing rate and low (0 Hz) to high (100 Hz) for baseline firing rate. e, Correlation analysis of behavioural tuning of all units analysed in lever, pellet and handling task (n = 5 mice; n = 38 neurons for lever-reach-tuned population, n = 30 neurons for pellet-reach-tuned population (Methods)). f, Summary scheme displaying population cotuning for latRM neurons during lever reaching and pellet reaching. By contrast, the handling-tuned latRM population is not engaged in reaching. Analysed neurons are not tuned to locomotion (swing phase). Grey shades, ±s.e.m.; **P<0.0025; ***P <0.00025; Wilcoxon non-parametric signed-rank test. Bonferroni correction was applied to account for multiple comparisons. In a, b, **P <0.01; ***P<0.001. Spearman's rank correlation test (e).

handling, an action phase that is behaviourally distinct from reaching (Fig. 1b). At the population level, action-ensemble cotuning for both reaching phases was significant, whereas we observed no significant cotuning or anticorrelation for either of these behaviours and food handling (Extended Data Fig. 2a–f). By contrast, we found that the handling-tuned latRM population is not recruited during the lever task or locomotion swing phases (Fig. 1b, Extended Data Fig. 2a). However, it is recruited with delay during the pellet task, in which reaching is followed by food handling. Thus, the handling-tuned latRM population is engaged during skilled forelimb behaviours that involve food handling. In agreement with the interpretation of action-specific tuning, the latRM population tuned to lever reaching was also recruited during pellet reaching, but not during the handling or locomotion swing phases (Extended Data Fig. 2b). These findings demonstrate that latRM neurons fractionate into distinct ensembles, which display behaviour-specific tuning within the forelimb action space (Fig. 1b, Extended Data Fig. 2f), and are unlikely to be recruited exclusively according to a muscular or receptive field map[23].

Skilled forelimb behaviours require latRM

To determine whether and which aspects of forelimb behaviours require latRM neurons for execution, we used loss-of-function tools in mice trained in forelimb reaching or food handling, two behaviours that recruit distinct latRM populations. We expressed the inhibitory designer receptor exclusively activated by designer drugs (DREADD) hM4Di, the activity of which can be regulated by systemic injection of clozapine N-oxide (CNO)[32] or—as a second tool—diphtheria toxin receptor (DTR), the expression of which, upon systemic injection of diphtheria toxin21, leads to neuronal ablation in the latRM of vGlut2cre (vGlut2 is also known as Slc17a6) mice (Extended Data Fig. 3a). We found no difference in open-field locomotor activity comparing conditions with or without CNO (Extended Data Fig. 3b). By contrast, forelimb reaching and food handling were severely affected in mice with chemogenetically silenced or ablated excitatory latRM neurons

(Fig. 2; Supplementary Videos 1, 2). First, we evaluated mice for their performance in the pellet task. We found a highly significant and reversible decline in the success rate to retrieve food pellets and place them in the mouth over baseline after injections of CNO, in vGlut2cre mice that had been injected with adeno-associated virus (AAV) encoding hM4Di (hereafter, latRM-hM4Di-vGlut2 mice) (Fig. 2b). The drop in success rate reflected a significant increase in the miss rate of the pellet by the forepaw during the reaching phase in CNO-injected latRM-hM4Di-vGlut2 mice

Fig. 2 | Excitatory latRM neurons are required for reaching and handling. a, Experimental design for food-pellet reaching assay, displaying mouse before reaching onset, during reaching and at target. b, Success rate for the same group of experimental (exp.) mice trained on pellet task (exp., n = 7 mice; control, n = 5 mice), displaying overall success rate (left) and success rate separately displayed by baseline recording day as well as two days each with the injection of CNO or phosphate-buffered saline (PBS) (right). c, Increased miss rate of food-pellet targeting upon CNO injections in latRM-hM4Di-vGlut2 mice (n = 7 mice). d, Point of maximal extension for reaching trajectories. Solid circles, average position of trials not missing the target; transparent circles, same measure for missed trials (each on days with PBS or CNO injection, respectively). e, Illustration of pasta-handling assay, displaying guide and grasp forepaw used in the handling task and the markings on pasta used for tracking of pasta position. f, Quantification of the number of pasta drops per behavioural session for latRM-hM4Di/DTR-vGlut2 mice without (control) or with (loss of function (LOF)) perturbation of excitatory latRM neurons. n = 7 mice for hM4Di; n = 3 mice for DTR. g, Quantification of percentage of time during which the preferred paw (as defined for the control condition) is used as guide paw. n = 7 mice for hM4Di; n = 3 mice for DTR. h, Fraction of time spent handling pasta at a given angle, relative to the preferred pasta angle for each mouse defined in the control session (set to 0 degrees) (Methods) shown for six representative mice (top) and average of all analysed (bottom) (n = 7 mice for hM4Di; n = 3 mice for DTR). Data are mean ± s.e.m. (b, c) and mean ± s.d. (f, g); Shades around mean denotes ±s.d. **P<0.01 ***P < 0.001, two-sided paired t-test (b, c) or Wilcoxon signed-rank test (f, g).

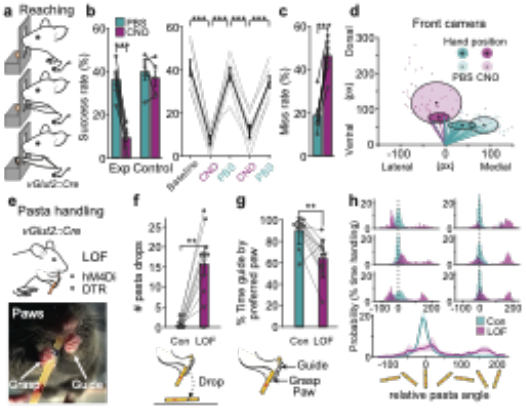

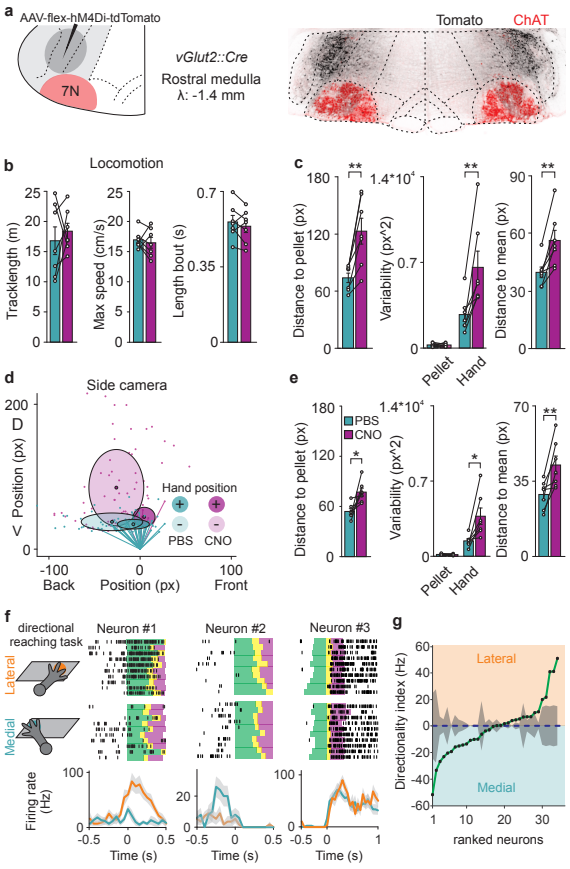

Extended Data Fig. 3 | Excitatory latRM neurons are required for precise directional reaching. a, Experimental scheme for injection of AAV-flex-hM4Di to the latRM of vGlut2cre mice and representative picture of targeting specificity for behavioural experiments, counterstained for ChAT. b, Attenuation of excitatory latRM neurons does not lead to defects in open field locomotion (track length, maximal speed and length of locomotor bouts), comparing PBS and CNO trials (n = 7 mice). c, Quantitative analysis of distance to food pellet, variability and distance to mean, separately shown for PBS and CNO trial days (front camera analysis, same mice as in Fig. 2; n = 7 mice). d, Analysis of point of maximal extension for reaching trajectories using a side camera for recordings (dark coloured circles: average position of trials not missing the target; light coloured circles: same measure for missed trials; each on days with PBS or CNO injection, respectively). e, Quantitative analysis of distance to food pellet, variability and distance to mean, separately shown for PBS and CNO trial days (side camera analysis; n = 7 mice). f, Experimental design for two-choice directional reaching task with lateral and medial reaching positions (left), three examples for recorded latRM neurons (right; n = 1 neuron each), each displaying single trials aligned to behavioural phases (green: reach; yellow: grasp; magenta: retract), spikes shown as lines (top), as well as average firing rates for lateral versus medial recorded trials (bottom). g, Quantification of directionality index (sorted from medial to lateral in ascending order, n = 34 neurons) for latRM neurons recorded during the two-choice directional reaching task. Data are mean ± s.e.m. (grey shades); *P< 0.05; **P <0.01; two-sided paired t-test.

(Fig. 2c). Reconstructions of the point of maximal extension of reaching trajectories showed that these mice consistently over-reached the pellet position and displayed significantly higher variability in end-point position (Fig. 2d, Extended Data Fig. 3c–e). Recording from latRM neurons during a two-choice reaching assay demonstrated that reaching-task-tuned latRM neurons line up along a spectrum of differential firing-rate changes comparing medial to lateral reaches

(Extended Data Fig. 3f, g). Our findings demonstrate that excitatory latRM neurons are essential during forelimb reaching for end-point targeting. In addition, some neurons exhibit signatures of reaching directionality, a property that has previously been observed in the cortex of monkeys and mice[19,33]. We next assayed the performance of latRM-hM4Di-vGlut2 mice or of vGlut2cre mice injected in the latRM with an AAV encoding DTR (hereafter, latRM-DTR-vGlut2 mice; referred to collectively as latRM-hM4Di/ DTR-vGlut2 mice) in pasta handling, a well-established paradigm for determining and quantifying the ability of rodents to manipulate food with their forepaws[34,35]. Rodents rarely drop the pasta piece and use stereotypical handling patterns[34,35], using a constant forepaw to guide the pasta into the mouth (guide paw) while the second paw grasps the pasta piece further away to stabilize it (grasp paw), together allowing for a relatively stable angle of the pasta (Fig. 2e, Supplementary Video 2). The latRM-hM4Di/DTR-vGlut2 mice exhibited severe pasta-handling defects, dropping pasta pieces significantly more frequently than during control sessions (Fig. 2f). We also found that latRM-hM4Di/ DTR-vGlut2 mice frequently switched hands during handling (Fig. 2g) and that pasta-angle stability was severely affected, which led to an overall broadening of the pasta-angle tuning curve owing to handling instability and hand switching (Fig. 2h, Extended Data Fig. 4a). However, despite these notable defects in

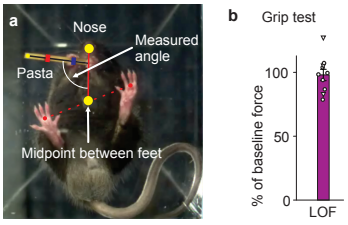

Extended Data Fig. 4 | Excitatory latRM neurons are required for pasta handling but not grip strength. a, Scheme explaining the approach to quantify pasta angle during handling. b, latRM-hM4Di/DTR-vGlut2 mice do not display defects in grip strength (n = 7 mice hM4Di and n = 3 mice DTR; data are mean ± s.e.m.).

pasta handling, latRM-hM4Di/ DTR-vGlut2 mice were not deficient in grip strength (Extended Data Fig. 4b), which suggests that the forelimb behavioural defects relate to the orchestrated use of

forepaws in manipulation. Together, these experiments demonstrate that excitatory latRM neurons are required for various aspects of skilled forelimb movements, as shown here for reaching and food handling.

Projection targets divide latRM neurons

The behavioural requirement and differential recruitment of excitatory latRM neurons in distinct phases of skilled forelimb movements raises the question of whether latRM neurons can be meaningfully stratified using anatomical and genetic approaches. We used anterograde tracing approaches with latRM-centred injections of AAV-flex-SynTag into vGlut2cre mice (Extended Data Fig. 5) to select three major termination regions for further analysis. These were the cervical spinal cord, the caudal medulla at the level of 10N and 12N (vagus and hypoglossal) motor neurons, and the contralateral latRM (Extended Data Fig. 5). We injected AAVs with retrograde targeting potential36 that conditionally express nuclear tags (retAAV-flex-nTag) into these downstream regions of vGlut2cre mice and mapped distribution of neurons retrogradely marked in the rostral medulla (Fig. 3a, Extended Data Fig. 6). We subdivided caudal medulla injections into medially (medullary reticular formation, ventral part (MdV)) and laterally (medullary reticular formation, dorsal part (MdD)) centred positions (Fig. 3a). We first compared neuronal distributions between the medial rostral medulla (medRM) and latRM. For spinally or MdV-projecting populations, about 80% of the neurons were located within the medRM and there was a high level of overlap between these populations (Extended Data Fig. 6). MdD-projecting neurons showed the opposite distribution profile, with around 80% residing in the latRM. Neurons projecting to the contralateral latRM were also dominant within the latRM (Extended Data Fig. 6). We next assessed the distribution patterns of the four retrogradely marked populations within the latRM. We observed a notable difference between spinally and MdD-projecting excitatory latRM neurons: the first population showed a dominant neuronal cluster immediately dorsal to the facial nucleus within the ventral parvicellular reticular nucleus. The latter exhibited a dorsally shifted cluster split

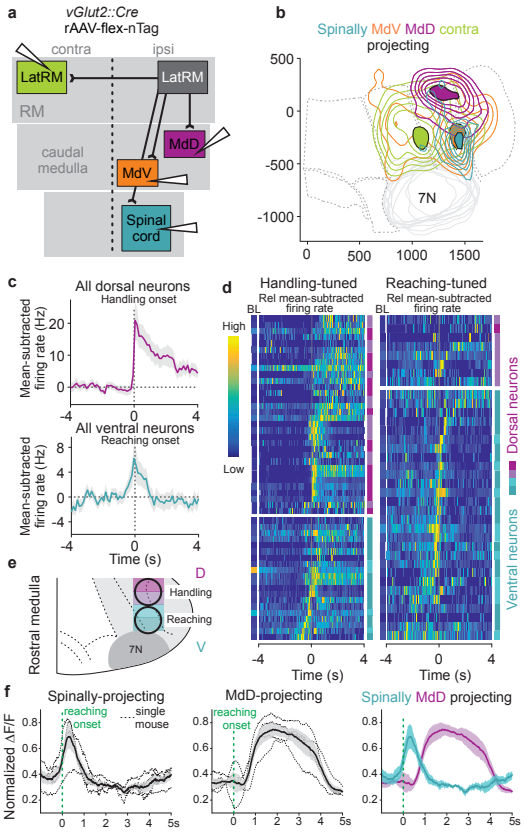

Fig. 3 | Differential tuning of latRM subpopulation to forelimb behaviours. a, Experimental design to analyse neuronal distribution of excitatory latRM neurons with projections to cervical spinal cord, the caudal medulla regions centred to MdV and MdD, and the contralateral (contra) latRM in vGlut2cre mice. Ipsi, ipsilateral. b, Density analysis of retrogradely marked neuronal cell bodies within the latRM upon injection in the four different downstream regions. Solid area marks the sites of highest sixth of density. c, d, Mean-subtracted firing rate of behaviourally tuned latRM neurons divided by dorsal (two shades of magenta) and ventral (two shades of cyan) recording sites during pellet task. c, Data depict average over all dorsal (top) (aligned to handling onset) or all ventral (bottom) (aligned to reaching onset) behaviourally tuned neurons. Neurons, n = 37 dorsal, n = 43 ventral. d, Raster plot depicts individual neurons tuned to handling (left) (aligned to handling onset) (n = 52) or reaching (right) (aligned to reaching onset) (n = 36), sorted by time of maximal relative mean-subtracted firing rate. Colour scales on the left depict low (0) to high (1) for relative mean-subtracted firing rate, and low (0 Hz) to high (100 Hz) for baseline firing rate. e, Summary diagram to illustrate that dorsal (D) recording sites encompass preferentially latRM neurons active during handling, whereas ventral (V) sites encompass latRM neurons active already during or before forelimb reaching. f, Fibre photometry data analysing the dynamics of calcium activity in excitatory latRM neurons retrogradely targeted from the cervical spinal cord (left, n = 4 mice), from MdD-centred injections (middle, n = 4 mice) and overlay of the two. Shades around mean denote ±s.e.m.

Extended Data Fig. 5 | Major synaptic targeting regions of excitatory latRM neurons. a, Analysis of synaptic output derived from excitatory latRM neurons in vGlut2cre mice to the cervical spinal cord, caudal medulla and contralateral latRM. Representative pictures (left; from one of three mice used for quantification in b) and reconstructions (middle) of SynTag puncta and synaptic density (right) plots for these output structures are shown. Scale bar, 250 µm. b, Quantification of synaptic numbers along the rostro-caudal axis of the cervical spinal cord (C1, C5 and C8). The decrease in synapses between rostral and caudal cervical spinal cord segments demonstrates that spinally projecting excitatory latRM neurons terminate more strongly in rostral cervical spinal cord segments compared to caudal counterparts (n = 3 mice, data are mean ± s.e.m.). c, Summary scheme of main synaptic output areas by excitatory latRM neurons.

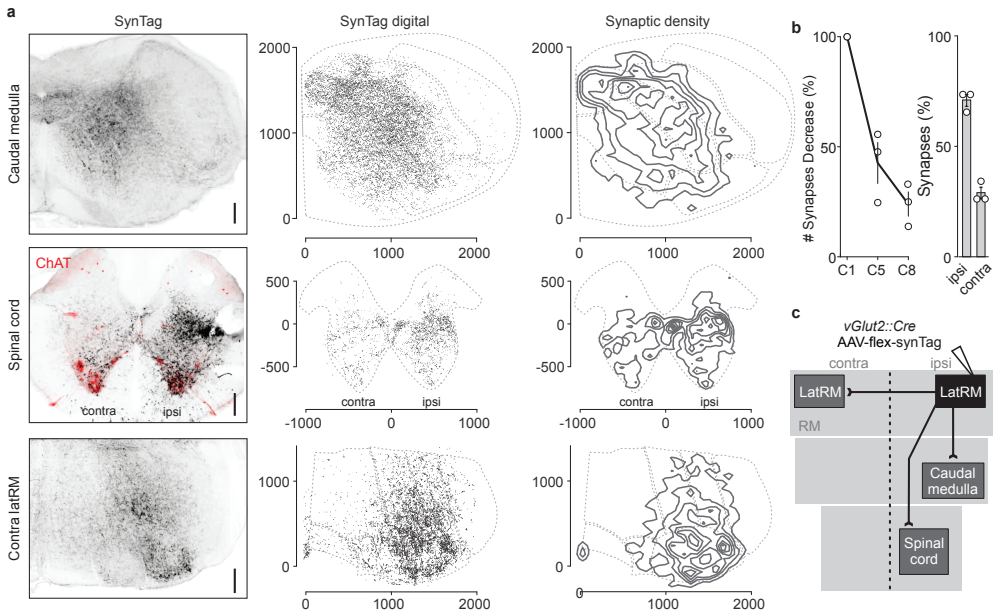

between the parvicellular reticular nucleus and the adjacent spinal trigeminal nucleus (Fig. 3b, Extended Data Fig. 6). MdV-projecting neurons were more evenly distributed within the latRM, but the highest neuronal density coincided with the spinally projecting population. Contralaterally projecting excitatory latRM neurons were also broadly distributed, but with a more medial location of the highest density (Fig. 3b, Extended Data Fig. 6). We determined the extent of overlap between spinally, MdV- and contralaterally projecting excitatory latRM neurons and found that the majority were anatomically separate (Extended Data Fig. 6). Much higher overlap was found within the medRM for spinally and MdV-projecting excitatory neurons, or when two retrograde viruses were co-injected into single target sites (Extended Data Fig. 6). Together, these findings demonstrate that— within the latRM—populations that are anatomically largely distinct and have different projection targets share a tight space, but exhibit spatial organization. Whereas spinally projecting latRM neurons reside most ventrally and MdD-projecting latRM neurons locate towards

the dorsal pole, MdV- and contralaterally projecting latRM neurons distribute more broadly throughout the territory (Fig. 3b, Extended Data Fig. 6).

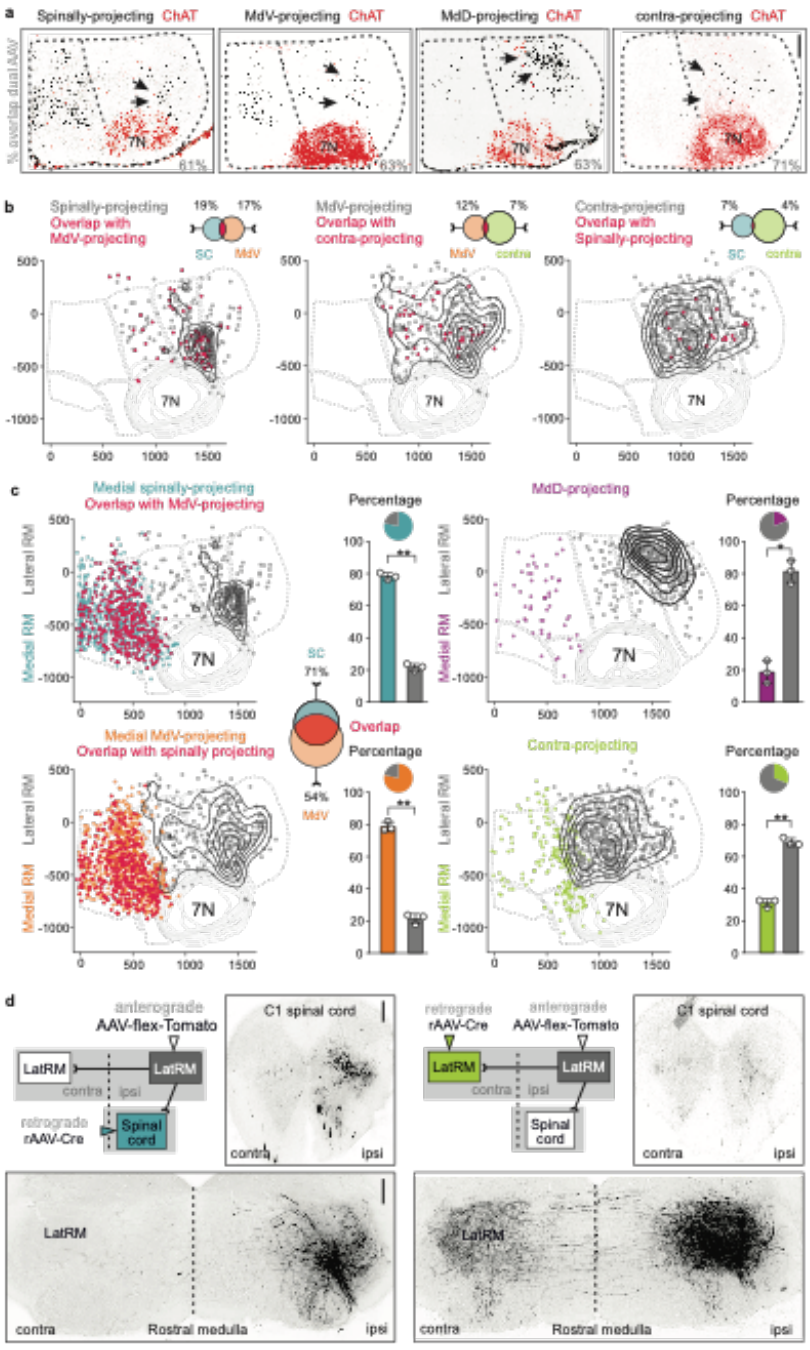

Extended Data Fig. 6 | Anatomical investigation of rostral medulla neurons on the basis of projections. a, Example pictures of retrogradely targeted excitatory latRM neurons from cervical spinal cord (from n = 3), MdV- (from n = 2), MdD- (from n = 2) or contralateral (from n = 3) latRM-centric injections counterstained with ChAT (red). Arrows point to cluster of neurons within the latRM, dotted vertical line depicts division between medRM and latRM. Numbers in grey shown in bottom right corner depict percentage overlap for co-injection of two retrograde AAVs into the corresponding output structure. Scale bar, 250 µm. b, Cellular overlap in

excitatory latRM neurons retrogradely marked from triple injections in the cervical spinal cord, centred in MdV and in contralateral latRM; representative example shown. There is a minor overlap between the three populations, as indicated by the Venn diagrams (n = 3 mice; dots: position of individual neurons; red dots: overlap with other displayed population; contour lines: density for distribution). c, Analysis of fractions of excitatory rostral medulla neurons residing in medRM versus latRM for four analysed populations shown in different colours (colour code as in Fig. 3, n = 3 mice from triple injections in the spinal cord, MdV-centric and contra latRM, n = 3 mice from MdD-centric), as well as overlap between excitatory medRM neurons retrogradely labelled from the cervical spinal cord and MdV-centric injections (red). d, Experiment combining retrograde targeting of latRM neurons with rAAV-Cre from the spinal cord (left; from n = 3 independent replicates) or contralateral latRM (right; from n = 2 independent replicates) with anterograde injections of AAV-flex-Tomato into ipsilateral latRM. Pictures demonstrate sparse projections of spinally projecting latRM neurons to contralateral latRM (left), and sparse projections of contralaterally projecting latRM neurons to the spinal cord (right), visualizing Tomato immunofluorescence. Scale bar, 250 µm. Data are mean ± s.e.m.; *P<0.05; **P<0.01; two-sided paired t-test.

Functional tuning in latRM populations

To determine whether neurons in the dorsal and ventral latRM exhibit differential neuronal activities during forelimb tasks, we acquired single-unit data along different dorsoventral latRM positions (Fig. 3c–e, Extended Data Fig. 7). Aligning behaviourally defined windows with neuronal activity, we found that reaching-tuned neurons were much more prevalent for ventral than dorsal latRM recording sessions.

Conversely, latRM neurons from dorsal recording positions exhibited a considerable bias towards handling tuning compared to reaching tuning (Fig. 3c–e, Extended Data Fig. 7). We next determined whether differential functional signatures in the dorsal and ventral latRM coincide with the activity of different populations stratified by axonal projection. We used retrograde viral injections to selectively target the expression of GCamp7s to excitatory latRM neurons projecting either to the spinal cord or the MdD, which reside mostly in ventral or dorsal latRM positions, respectively (Fig. 3f, Extended Data Fig. 8). We found that, whereas the signal of spinally projecting latRM neurons started to be upregulated before reaching, MdD-projecting populations showed preferential upregulation during handling after reaching (Fig. 3f, Extended Data Fig. 8). These findings demonstrate that, within the latRM, neurons tuned to the distinct forelimb subfunctions of reaching and handling map onto a dorsoventral axis aligned with their axonal projections.

Extended Data Fig. 7 | Analysis of activity along the dorsoventral axis in latRM. a, Experimental scheme depicting recording in dorsal versus ventral latRM during pellet task, with the focus on reaching versus food handling as behaviours (magenta shades: dorsal recording sites; cyan shades: ventral recording sites). b, Pellet-reach-tuned (left; n = 36) and handling-tuned (right; n = 52) latRM population ordered by peak time of respective behaviour onset. Dorsoventral recording position (4 depth) are indicated to the right of plot by a colour code. Bottom plots show average responses of all neurons as well as corresponding shuffled data. Colour scale depicts low (0) to high (1) for relative mean-subtracted firing rate and low (0 Hz) to high (100 Hz) for baseline firing rate; grey shades, ±s.e.m.; ***P <0.001; Wilcoxon non-parametric signed-rank test. Bonferroni correction was applied to account for multiple comparisons.

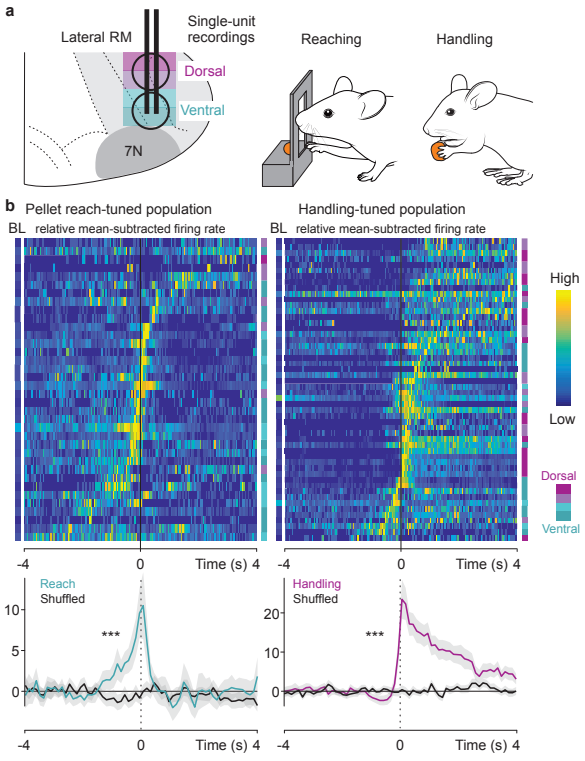

Extended Data Fig. 8 | Monitoring calcium activity from spinally and MdD-projecting latRM neurons. a, Fibre photometry data analysing the dynamics of calcium activity in excitatory latRM neurons retrogradely targeted from the cervical spinal cord (n = 4 mice) and from MdD-centred injections (n = 4 mice). Traces are aligned relative to handling onset (dotted line). Shades around mean of individual mice are ±s.e.m. b, Average of mean dynamics of calcium activity for neurons shown in a during onset of locomotion trials (running, n = 4 mice MdD-centred projections, n = 3 mice spinal cord projections) or shuffled data (aligned to reaching onset, n = 4 mice MdD centred projections, n = 4 mice spinal cord projections). Shades around mean of individual mice are ±s.e.m.

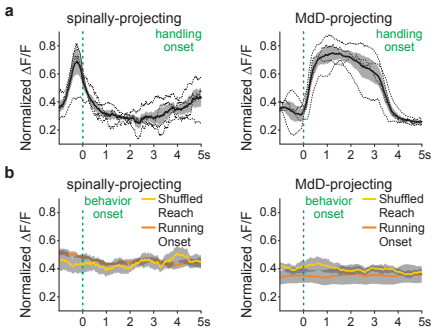

LatRM neurons elicit forelimb behaviours

We next asked whether and what kind of behaviour can be induced by optogenetic stimulation of the excitatory latRM neuron populations identified by axonal targets. To contrast these latRM-centred experiments, we also probed spinally projecting medRM neurons. We targeted rostral medulla neurons retrogradely using retAAV-(flex)-FLP-V5 injections in the different downstream targets of vGlut2cre mice and injected a dual-recombinase activated AAV37 expressing ReaChR into the rostral medulla with optic-fibre placement dorsal to the previously mapped highest neuronal density (Fig. 4a, Extended Data Fig. 9a). To quantify the repertoire of behaviours elicited in these optogenetic stimulation experiments, we charted their nature and reliability for individual mice (Fig. 4b–d). We found that individual mice express stable behavioural phenotypes at high reliabilities (Fig. 4d). Moreover, the nature of the expressed phenotype was linked to the identity of the downstream target of the studied neuronal population, but we observed further behavioural diversity for experiments targeting MdVor MdD-projecting latRM neurons. Optogenetic stimulation of spinally projecting excitatory latRM neurons induced unilateral forelimb reaching, but not more-complex forelimb movements that involve digit flexure (Fig. 4b–d, Extended Data Fig. 9, Supplementary Video 3). Electromyographic recordings from biceps and triceps forelimb muscles showed that the same muscle-activation sequence occurred during naturally executed and optogenetically induced forelimb reaching—albeit that the latter occurred at a faster time scale38 (Extended Data Fig. 10). Moreover, although this was challenging owing to the freely moving nature of our experiments, analysis of reaching-trajectory end points showed higher similarity between trials of one mouse than to the trials of other mice (Fig. 4c, Extended Data Fig. 9b), which possibly indicates that the precise composition of the optogenetically targeted ensemble is instrumental for behavioural nuances between mice.

Fig. 4 | Stimulation of latRM populations elicits specific forelimb movements. a, Left, injection scheme for experimental design to optogenetically stimulate excitatory latRM neurons projecting to different downstream targets. Neurons were retrogradely targeted through spinal cord injections, MdV- or MdD-centred injections in the caudal medulla or contralateral latRM-centred injections of rAAV-(flex)FLP in vGlut2cre mice, combined with ipsilateral latRM-centred injections of AAV-ConFon-ReaChR to target latRM neurons co-expressing Cre and FLP. Right, summary diagram displays the alignment between identity of excitatory latRM neuron population by projection target and observed behaviours. The stimulation of latRM neurons that engage circuits in the caudal medulla elicits more-complex forelimb movements involving digits than those elicited by stimulation of excitatory latRM neurons that directly engage spinal circuits. b, Spatiotemporal analysis of optogenetically induced movements using DeepLabCut. Data depict example pictures from movies of different behaviours as indicated, including DeepLabCut-tracked positions (red dots). c, Average trajectories of DeepLabCut-tracked, optogenetically induced reaching (left) (n = 4 mice), tapping (middle) (n = 3 mice) and grooming (right) (n = 2 mice). Solid and dotted lines indicate the trajectory of the ipsi- and contralateral forelimb during grooming respectively. d, Chart displaying behavioural repertoire of mice included in the optogenetic stimulation data set. Mouse identifier (ID) on the left is stratified by injection sites for retrograde (retro) (rAAV-(flex)FLP) and anterograde (AAV-ConFon-ReaChR) AAVs. Vertical columns depict observed behaviours, using a colour scale for behavioural reliability (0–100%) and summing up to 100% for all columns. antero, anterograde; bi, bilateral; c, contralateral; i, ipsilateral.

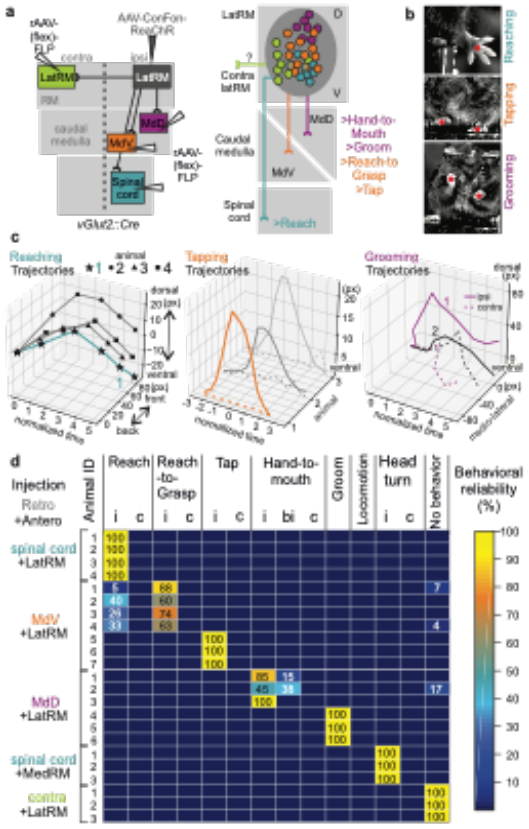

Stimulation of MdV-projecting latRM neurons elicited ipsilateral reach-to-grasp movements in a fraction of mice, characterized by the supplementation of induced reaches by digit flexing and/or grasping, or ipsilateral forelimb tapping movements, in the remaining mice of this category (Fig. 4b–d, Extended Data Fig. 9b, Supplementary Video 3). By contrast, the stimulation of MdD-projecting latRM neurons produced hand-to-mouth movements or grooming (Fig. 4b–d, Extended

Data Fig. 9, Supplementary Video 3). The stimulation of contralaterally projecting excitatory latRM neurons did not induce obvious movements (Fig. 4d, Extended Data Fig. 9, Supplementary Video 3). Notably, whereas the behaviours elicited by stimulation of latRM subpopulations all involved forelimb use, the stimulation of medially located spinally projecting medRM neurons induced head-turning that was ipsilateral to implantation (Fig. 4d, Supplementary Video 3).

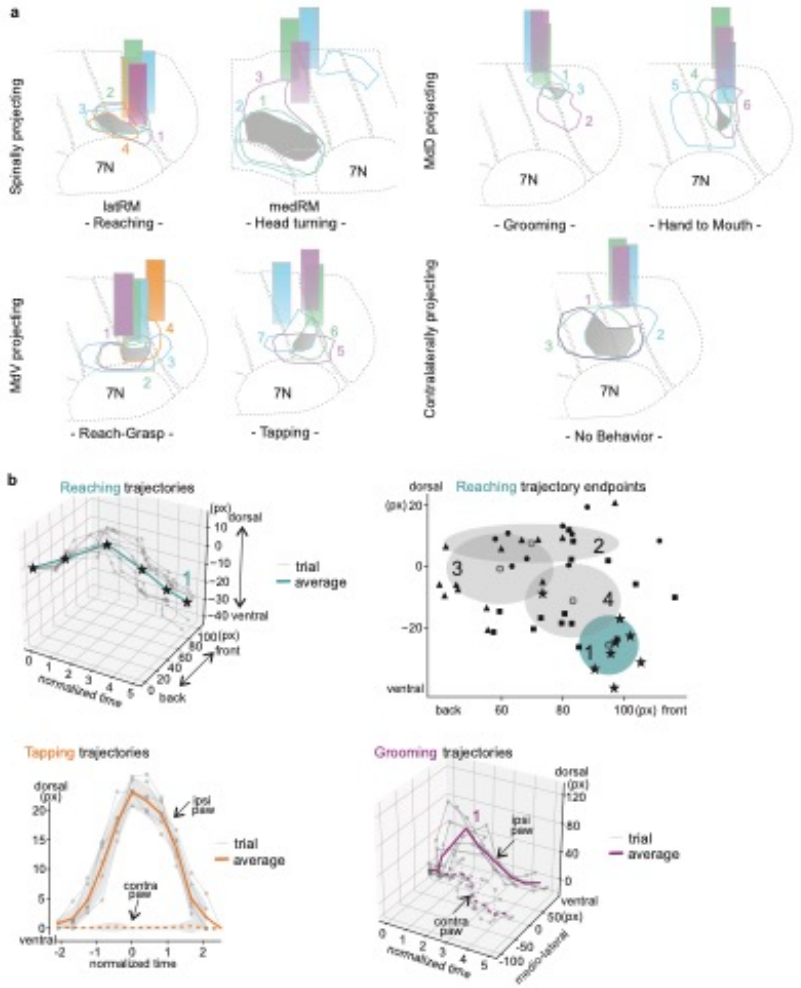

Extended Data Fig. 9 | Optogenetic activation of rostral medulla subpopulations. a, Reconstruction of fibre placements and local virus expression sites at the rostral medulla level. Each colour corresponds to one mouse included in the analysis shown in Fig. 4 (code corresponds to mouse ID number shown in Fig. 4d). b, Spatiotemporal analysis of optogenetically induced movements using DeepLabCut. Data depict reaching trajectories (top, left) of different stimulation trials (grey lines) in one mouse (average: cyan), and the lateral view of the trajectory endpoints of reaching mice shown in Fig. 4c using a side-camera (top, right) (Methods). Trajectories of different stimulation trials reconstructed for forepaws ipsi- and contralateral to stimulation during optogenetically-induced tapping (bottom left; average: orange; grey shade, ±s.d.) or grooming (bottom right; average: purple) are also shown.

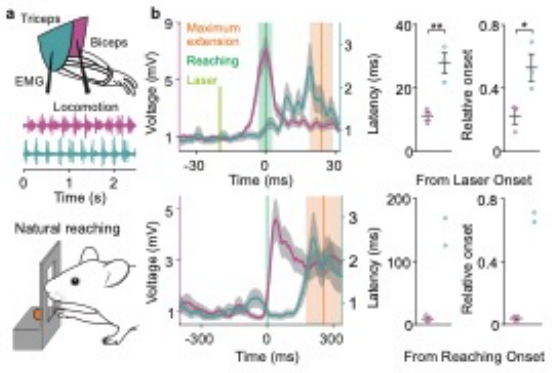

Extended Data Fig. 10 | Stimulation of spinally projecting excitatory latRM neurons recruits forelimb muscles in a sequence resembling natural reaching. a, Scheme depicting implantation of EMGs into forelimb biceps and triceps muscles, and raw signal demonstrating that these muscles are active in alternation during natural locomotion (below), according to their flexor (biceps) and extensor (triceps) function. b, EMG recordings and quantification (latency and relative onset) for biceps and triceps recordings during optogenetically induced reaching by stimulation of spinally projecting excitatory latRM neurons (top; n = 3 mice for biceps and triceps) or natural reaching (bottom; 0 = reaching onset; n = 3 mice for biceps and n = 2 mice for triceps). Grey shades, ±s.e.m.; *P <0.05; **P <0.01; two-sided paired t-test.

These findings suggest a mediolateral segregation of neuronal substrates for head turning and forelimb movements within the rostral medulla in mice; this is perhaps distinct from cats, in which both elements seem to be located rather medially[39]. Finally, optogenetic stimulations of excitatory latRM neurons targeted by direct injection into the latRM elicited only simple, ipsilateral forelimb movements that included reaching and tapping-like behaviours (Supplementary Video 3). Thus, the successful production of behavioural diversity by latRM neurons is critically dependent on the specific latRM ensemble that is targeted for optogenetic stimulation experiments through its distinct axonal projections. Whether these latRM populations also exhibit differential roles in the execution of natural forelimb behaviours awaits the generation of viral tools for more-complete retrograde targeting than is currently possible.

Discussion

The use of forelimbs to access and manipulate objects in the environment is one of the most essential additions to the movement repertoire that arose in limbed animals, and it encompasses behavioural phases and attributes that are evolutionarily conserved from rodents to humans[7,20,40]. Our work describes the latRM of the brainstem as a critical orchestrator in the execution of skilled forelimb movements. Here we discuss models of how complex, skilled forelimb movements may be regulated by the combinatorial use of specific brainstem-to-spinal cord and intra-brainstem circuits. We found that latRM neurons divide into at least four anatomically distinct populations by axonal targets. The initiation of most skilled forelimb movements requires the transport of one or both hands to the site of action (commonly referred to as forelimb reaching). Optogenetic stimulation of the spinally projecting latRM subpopulation elicits unilateral reaching. In agreement with this, latRM neurons exhibit preferential projections to the ipsilateral rostral cervical spinal cord, which contains circuits for the control of proximal forelimb muscles. Notably, latRM neurons with direct spinal projections are not sufficient to elicit forelimb movements that are more complex than reaching. Excitatory latRM neurons projecting to the caudal medulla signal and can generate diverse and complex forelimb movements, which involve the use of digits during grasping and/or action bilateralization during grooming or hand-to-mouth movements. These diverse forelimb behaviours are stably expressed in individual mice in a 'winner-take-it-all' fashion, probably owing to the targeting of specific neuronal ensembles through retrograde axonal infection (which is instrumental for obtaining behavioural diversity through optogenetic probing). Caudal medullary neurons then establish functional links to the caudal cervical spinal cord essential for generating distal forelimb movements[21], which probably involve propriospinal neurons with direct connections to motor neurons[7,12].

Our work uncovers the existence and organization of brainstem circuits that encompass task- and action-phase-selective neuronal ensembles in the rostral medulla. Notably, shared latRM

neuronal ensembles are engaged during related forelimb actions (that is, reaching in different forelimb behaviours), whereas distinct ensembles are used for dissimilar forelimb movements (that is, reaching versus food handling). No significant encoding in the latRM is observed for locomotion. The circuit elements described here are, therefore, non-overlapping with pathways that implement full-body movements including locomotion[2–4,41], which engages the same muscles but in an entirely different task and context. These findings resonate with recent work in the striatum, in which closer actions are also encoded by overlapping neuronal ensembles whereas distant actions engage distinct ensembles[42–44]. In the striatum, these ensembles are found in common overall space, whereas our findings demonstrate that the anatomical demixing of signals for locomotion and skilled forelimb movements has occurred within brainstem circuits. The brainstem neuronal populations we identify here are in a prime position to integrate cortical and other brain-wide signals and transmit them for precise forelimb execution to the spinal cord. Even beyond its role in execution of forelimb movements, the lateral brainstem is a complex integration hub for higher motor centres that are also engaged in regulating orofacial behaviours[16,18,45–47], which suggests additional integration and coordination in this area. The discovery that neuronal segregation by task specificity in action space exists in the most caudal part of the brain, and that the identified brainstem neurons together are needed to implement different aspects of skilled forelimb movements, provides a deep understanding of how body actions that use limbs are regulated through the engagement of dedicated neuronal circuits.

References

1. Ferreira-Pinto, M. J., Ruder, L., Capelli, P. & Arber, S. Connecting circuits for supraspinal control of locomotion. Neuron 100, 361–374 (2018).

2. Roseberry, T. K. et al. Cell-type-specific control of brainstem locomotor circuits by basal ganglia. Cell 164, 526–537 (2016).

3. Caggiano, V. et al. Midbrain circuits that set locomotor speed and gait selection. Nature 553, 455–460 (2018).

4. Capelli, P., Pivetta, C., Soledad Esposito, M. & Arber, S. Locomotor speed control circuits in the caudal brainstem. Nature 551, 373–377 (2017).

5. Bouvier, J. et al. Descending command neurons in the brainstem that halt locomotion. Cell 163, 1191–1203 (2015).

6. Lemon, R. N. Descending pathways in motor control. Annu. Rev. Neurosci. 31, 195–218 (2008).

7. Alstermark, B. & Isa, T. Circuits for skilled reaching and grasping. Annu. Rev. Neurosci. 35, 559–578 (2012).

8. Klaus, A., Alves da Silva, J. & Costa, R. M. What, if, and when to move: basal ganglia circuits and self-paced action initiation. Annu. Rev. Neurosci. 42, 459–483 (2019).

9. Peters, A. J., Liu, H. & Komiyama, T. Learning in the rodent motor cortex. Annu. Rev. Neurosci. 40, 77–97 (2017).

10. Wang, X. et al. Deconstruction of corticospinal circuits for goal-directed motor skills. Cell 171, 440–455 (2017).

11. Azim, E., Jiang, J., Alstermark, B. & Jessell, T. M. Skilled reaching relies on a V2a propriospinal internal copy circuit. Nature 508, 357–363 (2014).

12. Pivetta, C., Esposito, M. S., Sigrist, M. & Arber, S. Motor-circuit communication matrix from spinal cord to brainstem neurons revealed by developmental origin. Cell 156, 537–548 (2014).

13. Grillner, S., Georgopoulos, A. P. & Jordan, L. M. in Neurons, Networks, and Motor Behavior (eds Stein P. S. G. et al.) 3–19 (The MIT Press, 1997).

14. Arber, S. & Costa, R. M. Connecting neuronal circuits for movement. Science 360, 1403–1404 (2018).

15. Grillner, S. Biological pattern generation: the cellular and computational logic of networks in motion. Neuron 52, 751–766 (2006).

16. Ruder, L. & Arber, S. Brainstem circuits controlling action diversification. Annu. Rev. Neurosci. 42, 485–504 (2019).

17. Kim, L. H. et al. Integration of descending command systems for the generation of context-specific locomotor behaviors. Front. Neurosci. 11, 581 (2017).

18. Svoboda, K. & Li, N. Neural mechanisms of movement planning: motor cortex and beyond. Curr. Opin. Neurobiol. 49, 33–41 (2018).

19. Georgopoulos, A. P., Kalaska, J. F., Caminiti, R. & Massey, J. T. On the relations between the direction of two-dimensional arm movements and cell discharge in primate motor cortex. J. Neurosci. 2, 1527–1537 (1982).

20. Iwaniuk, A. N. & Whishaw, I. Q. On the origin of skilled forelimb movements. Trends Neurosci. 23, 372–376 (2000).

21. Esposito, M. S., Capelli, P. & Arber, S. Brainstem nucleus MdV mediates skilled forelimb motor tasks. Nature 508, 351–356 (2014).

22. Schepens, B. & Drew, T. Descending signals from the pontomedullary reticular formation are bilateral, asymmetric, and gated during reaching movements in the cat. J. Neurophysiol. 96, 2229–2252 (2006).

23. Schepens, B., Stapley, P. & Drew, T. Neurons in the pontomedullary reticular formation signal posture and movement both as an integrated behavior and independently. J. Neurophysiol. 100, 2235–2253 (2008).

24. Soteropoulos, D. S., Williams, E. R. & Baker, S. N. Cells in the monkey ponto-medullary reticular formation modulate their activity with slow finger movements. J. Physiol. (Lond.) 590, 4011–4027 (2012).

25. Lawrence, D. G. & Kuypers, H. G. The functional organization of the motor system in the monkey. I. The effects of bilateral pyramidal lesions. Brain 91, 1–14 (1968).

26. Lemon, R. N., Landau, W., Tutssel, D. & Lawrence, D. G. Lawrence and Kuypers (1968a, b) revisited: copies of the original filmed material from their classic papers in Brain. Brain 135, 2290–2295 (2012).

27. Lawrence, D. G. & Kuypers, H. G. The functional organization of the motor system in the monkey. II. The effects of lesions of the descending brain-stem pathways. Brain 91, 15–36 (1968).

28. Ross, G. S. & Sinnamon, H. M. Forelimb and hindlimb stepping by the anesthetized rat elicited by electrical stimulation of the pons and medulla. Physiol. Behav. 33, 201–208 (1984).

29. Franklin, K. B. & Paxinos, G. The Mouse Brain in Stereotaxic Coordinates, 3rd edn (Elsevier, 2007).

30. Xu, T. et al. Rapid formation and selective stabilization of synapses for enduring motor memories. Nature 462, 915–919 (2009).

31. Jin, X. & Costa, R. M. Start/stop signals emerge in nigrostriatal circuits during sequence learning. Nature 466, 457–462 (2010).

32. Roth, B. L. DREADDs for neuroscientists. Neuron 89, 683–694 (2016).

33. Galiñanes, G. L., Bonardi, C. & Huber, D. Directional reaching for water as a cortex-dependent behavioral framework for mice. Cell Rep. 22, 2767–2783 (2018).

34. Tennant, K. A. et al. The vermicelli and capellini handling tests: simple quantitative measures of dexterous forepaw function in rats and mice. J. Vis. Exp. (41):2076 (2010).

35. Whishaw, I. Q. et al. The syntactic organization of pasta-eating and the structure of reach movements in the head-fixed mouse. Sci. Rep. 7, 10987 (2017).

36. Tervo, D. G. et al. A designer AAV variant permits efficient retrograde access to projection neurons. Neuron 92, 372–382 (2016).

37. Fenno, L. E. et al. Targeting cells with single vectors using multiple-feature Boolean logic. Nat. Methods 11, 763–772 (2014).

38. Yakovenko, S., Krouchev, N. & Drew, T. Sequential activation of motor cortical neurons contributes to intralimb coordination during reaching in the cat by modulating muscle synergies. J. Neurophysiol. 105, 388–409 (2011).

39. Drew, T. & Rossignol, S. Functional organization within the medullary reticular formation of intact unanesthetized cat. I. Movements evoked by microstimulation. J. Neurophysiol. 64, 767–781 (1990).

40. Whishaw, I. Q., Pellis, S. M. & Gorny, B. P. Skilled reaching in rats and humans: evidence for parallel development or homology. Behav. Brain Res. 47, 59–70 (1992).

41. Shik, M. L. & Orlovsky, G. N. Neurophysiology of locomotor automatism. Physiol. Rev. 56, 465–501 (1976).

42. Barbera, G. et al. Spatially compact neural clusters in the dorsal striatum encode locomotion relevant information. Neuron 92, 202–213 (2016).

43. Klaus, A. et al. The spatiotemporal organization of the striatum encodes action space. Neuron 96, 949 (2017).

44. Parker, J. G. et al. Diametric neural ensemble dynamics in parkinsonian and dyskinetic states. Nature 557, 177–182 (2018).

45. Petersen, C. C. H. Sensorimotor processing in the rodent barrel cortex. Nat. Rev. Neurosci. 20, 533–546 (2019).

46. Han, W. et al. Integrated control of predatory hunting by the central nucleus of the amygdala. Cell 168, 311–324 (2017).

47. Mercer Lindsay, N. et al. Orofacial movements involve parallel corticobulbar projections from motor cortex to trigeminal premotor nuclei. Neuron 104, 765–780.e3 (2019).

48. Vong, L. et al. Leptin action on GABAergic neurons prevents obesity and reduces inhibitory tone to POMC neurons. Neuron 71, 142–154 (2011).

49. Takeoka, A., Vollenweider, I., Courtine, G. & Arber, S. Muscle spindle feedback directs locomotor recovery and circuit reorganization after spinal cord injury. Cell 159, 1626–1639 (2014).

50. Dana, H. et al. High-performance calcium sensors for imaging activity in neuronal populations and microcompartments. Nat. Methods 16, 649–657 (2019).

51. Basaldella, E., Takeoka, A., Sigrist, M. & Arber, S. Multisensory signaling shapes vestibulo-motor circuit specificity. Cell 163, 301–312 (2015).

52. Armbruster, B. N., Li, X., Pausch, M. H., Herlitze, S. & Roth, B. L. Evolving the lock to fit the key to create a family of G protein-coupled receptors potently activated by an inert ligand. Proc. Natl Acad. Sci. USA 104, 5163–5168 (2007).

53. Miri, A. et al. Behaviorally selective engagement of short-latency effector pathways by motor cortex. Neuron 95, 683–696 (2017).

54. Botev, Z. I., Grotowski, J. F. & Kroese, D. P. Kernel density estimation via diffusion. Ann. Stat. 38, 2916–2957 (2010).

55. Mathis, A. et al. DeepLabCut: markerless pose estimation of user-defined body parts with deep learning. Nat. Neurosci. 21, 1281–1289 (2018).

56. Nath, T. et al. Using DeepLabCut for 3D markerless pose estimation across species and behaviors. Nat. Protocols 14, 2152–2176 (2019).

Methods

No statistical methods were used to predetermine sample size. The experiments were not randomized, and investigators were not blinded to allocation during experiments and outcome assessment.

Mice

We used vGlut2cre mice (RRID: IMSR_JAX:028863)48 maintained on a mixed genetic background (129/C57Bl6). Experimental mice originating from different litters were used in individual experiments. No criteria were applied to allocate mice to experimental groups, and mice had marks for unique identification. For all behavioural experiments, we used 2–4-month-old heterozygous males, backcrossed to C57Bl6. For anatomical experiments, both male and female mice were used. Mice were maintained on a 12-h light–dark cycle in a temperature (22 ± 1 °C) and humidity controlled (45–65%) environment. Housing, surgery procedures, behavioural experiments and euthanasia were performed in compliance with the Swiss Veterinary Law guidelines.

Virus production, injections and implantations

We used the following previously described AAVs, all based on a backbone derived from Allen Brain (AAV-CAG-flex-tdTomato-WPRE-bG H): AAV-flex-SynGFP12 and AAV-flex-SynMyc49 (referred to as AAV-flex-SynTag), AAV-flex-DTR21 as well as AAV-flex-Flp-H2B-V5 and AAV-H2B-10×Myc[4]. Viral constructs that have not previously been reported were designed by analogy with the above constructs: AAV-flex-H2B-GFP, AAV-flex-H2B-TdTomato, AAV-flex-H2B-V5 (last three AAVs commonly referred to as AAV-flex-nTag), AAV-flex-hM4Di-Tomato, AAV-flex-GCaMP7s50 and AAV-Flp-H2B-V5. The AAV-ConFon-ReaChR-Citrine-YFP construct was created using a previously described strategy[37]. To infect neuronal cell bodies but not axons, a serotype plasmid 2.9 was used as in previous studies[12,21,51]. For retrograde labelling by means of

axonal infection, a rAAV2-retro capsid plasmid[36] was used for coating as previously described[4]. AAVs used in this study were of genomic titres >1 × 10^{13} and produced following standard protocols. Viruses were injected into the brainstem with high-precision stereotaxic instruments (Kopf Instruments, Model 1900) under isoflurane anaesthesia as previously described[4,21]. Viral injections in the spinal cord were targeted to the cervical spinal cord comprising spinal segments C1–C5 (approximate injection volume of 300–500 nl). The following coordinates were used to target the investigated brainstem regions referenced with lambda as the point of origin for anterior–posterior (AP), mediolateral (ML) and dorsoventral (DV) axes (approximate injection volumes of 50–100 nl): latRM (−1.4; ±1.55; −4.8 (AP; ML; DV; in mm)); MdV (−3.0; ±0.6; −5.5); MdD (−3.0; ±1.4; −5.3); latRM dorsal (−1.4; ±1.55; −4.3); and medRM (−1.4; ±0.5; −4.8). To map output projections of excitatory latRM neurons, we injected AAV-flex-SynTag and waited more than two weeks for expression. Retrograde tracings of latRM outputs using retro-flex-nTag viruses were carried out by injections in the spinal cord before brainstem injections. After the final injection, we waited for over ten days. Triple injections were performed for the combination of spinal cord, MdV and the contralateral latRM. MdD injections were performed in separate experiments. For co-injections into single target regions, viruses were mixed before injection. Injections to bilaterally target excitatory latRM neurons for loss-of-function experiments were carried out more than two weeks before baseline reaching-success rates were assessed or handling proficiency was assayed, to allow for sufficient time for expression of hM4Di. CNO (Tocris, cat. no. 4936) was injected intraperitoneally at 10 mg per kg body weight in PBS to initiate attenuation of neuronal firing upon interaction with the hM4Di receptor3,52. For mice expressing DTR in excitatory latRM neurons, diphtheria toxin (Sigma D0564) was administered intraperitoneally (100 ng per g body weight) after baseline behaviours were recorded. For optogenetic activation of selected neuronal subpopulations, injections involving the cervical spinal cord were conducted first, as described for anatomical experiments and using retro-(flex)-Flp-H2B-V5. Subsequently, the latRM was injected unilaterally with AAV-ConFon-ReaChR-Citrine-

YFP and an optic fibre was implanted 200 µm above the injection site (diameter of 200 µm, MFC_200/230-0.48_6mm_ZF1.25_FLT Mono Fibreoptic Cannula; Doric lenses). For all other subpopulations stratified by projections involving targets in the brainstem (contralateral latRM, MdV and MdD), injections and implantations were targeted only to the brainstem. For fibre photometry experiments, the optic fibre was implanted 100 µm above the neuronal population of interest (diameter of 200 µm, MFC_200/230- 0.48_6mm_ZF1.25_FLT Mono Fibreoptic Cannula; Doric lenses). For electrophysiological recordings, single-shank chronic 16-channel or dual-shank chronic 32-channel silicon probes were implanted (Cambridge NeuroTech, P-series, 6 mm length). These were mounted on a nanodrive (Cambridge NeuroTech) allowing for sequential recordings at different depths and implanted in the latRM (AP and ML coordinates as for virus injections) at a dorsal–ventral depth of around −3.0 mm using light curable cement (Relyx Unicem 2, 3M). Stimulation experiments were started over two weeks after injection and implantation. We assessed injection sites after termination of experiments by using ChAT immunohistochemistry (as described in 'Immunohistochemistry and microscopy') to visualize motor nuclei. For electrophysiological recordings, we also visualized the site of electrical lesion at the end of the recordings to confirm correct probe placement. The mouse brain atlas was used as reference for determining the spatial injection specificity of the viral labelling29. For optogenetic activation experiments with latRM and medRM subpopulations, we mapped fibre placement as well as the extent of targeted neurons at injection sites. Only mice with confirmed anatomical precision were included in the subsequent analysis. The region here referred to as the latRM combines sites of the brainstem regions indicated as intermediate reticular nucleus, parvicellular reticular nucleus and spinal trigeminal nucleus[29] in the rostral part of the medulla spanning the rostro-caudal extent of the facial motor nucleus (7N). The rostro-caudally aligned region medial to latRM is referred to as medRM. For MdV and MdD nomenclature, we followed the boundaries delineated in the mouse brain atlas[29].

Electrophysiological recordings

Following surgery (as described in 'Virus production, injections and implantations'), the probe was lowered during subsequent days to the starting position in the latRM. After every recording session, the probe was lowered by 100–200 µm to record along the dorso-ventral axis of the latRM to finally reach the position in the facial nucleus (7N, DV: −5.0 mm from the brain surface) on the last experimental day. For recordings specifically focusing on DV position analysis, the electrode was lowered in steps of 200 µm, spanning the latRM DV axis in four steps (the first two grouped as dorsal indicated by shades of magenta and second two grouped as ventral indicated by shades of cyan in the corresponding figure panels). Electrical lesions (3 s at 200 µA) shortly before perfusions were performed to confirm recording locations (Extended Data Fig. 1) using an electrical stimulator (WPI, Stimulus isolator A360). The extracellular signal was amplified and acquired at 40 kHz using a commercially available soft- and hardware recording system (OmniPlex, Plexon). Filtered, continuous data from each recording session consisting of all behavioural tasks carried out within this session were grouped into adjacent, fictive tetrodes and sorted manually in tetrode mode, using commercially available software (Offline Sorter v.3.3.5, Plexon). Autocorrelation, high relative signal-to-noise ratios as well as waveform comparison were used to ensure high-quality data using commercially available software (NeuroExplorer v.5, Plexon) (Extended Data Fig. 1e). Further cross-correlation between channels ensured the elimination of units recorded at multiple recording sites. For recordings comparing multiple behaviours (as described in 'Behavioural experiments'), we recorded a total of 243 neurons in the lever task, 212 neurons during pellet reaching and handling and 198 neurons during open field behaviour, totalling 246 neurons across all behaviours and 194 neurons that were stable and reliably present across all behaviours in 5 mice (Extended Data Fig. 1a). For recordings assessing differential encoding along the dorsoventral axis and distinct response properties depending on mediolateral reaching direction (as described in 'Behavioural experiments'), we recorded a total

of 144 neurons in 2 mice. Sorted, single-unit data and spiking time points were used for further analysis on other freely moving behaviours (as described in 'Behavioural experiments' and 'Behavioural analysis, scripts and statistics').

Electromyographic recordings

For electromyographic (EMG) recordings during stimulation of spinally projecting latRM neurons, injections and fibre implantation were conducted as described in 'Virus production, injections and implantations'. Cable preparation and EMG implantation of the biceps and triceps muscle were conducted as previously reported53. Acquisition was carried out either in response to optogenetic stimulation (as described in 'Optogenetic activation experiments') or during pellet reaching (as described in 'Pellet reaching task'). The signal was amplified and bandpass-filtered (A-M systems 1700, gain 100, bandpass 100–1,000 Hz) and acquired using a Plexon recording system (Omniplex, Plexon) at 5,000 Hz. We subsequently applied a mean subtraction to correct for the DC offset.

Photometry recordings

Recordings of calcium activity started two weeks after surgery, using a multi-fibre photometry system (CineLyzer, Plexon). Implants were connected to the system through a customized patch cord (Doric Lenses) to simultaneously allow for delivery of excitation light (470 nm Plexon) and collection of GCaMP emission at 60 Hz. A continuous excitation intensity of 30–40 µW was used for all experiments, measured as described in 'Optogenetic activation experiments'. Experimental sessions were repeated to collect at least ten successful, first-reaching trials, as describing in 'Pellet task' in 'Behavioural experiments').

Immunohistochemistry and microscopy

Immunohistochemistry to visualize virally expressed transgenes was performed on all mice used in this study. This included mice from anatomical and behavioural experiments. Mice were

anaesthetized using a ketamine–xzylazine solution before transcardial perfusion with cold PBS and subsequent fixation using a 4% paraformaldehyde (PFA) solution (Sigma). Brains and spinal cords were carefully dissected and post-fixated with PFA for over 8 h following perfusion. To cryopreserve the tissue, we incubated brains and spinal cord in a 30% sucrose w/v in PBS solution for at least one day. We cut 80-µm-thick slices on a cryostat, collected sections sequentially into individual wells (coronally for brain tissue and transversely for spinal cord). Following a one-hour incubation in blocking solution (1% BSA/0.2% TritonX100/PBS), we added primary antibodies diluted in blocking solution for 1–3 days of incubation at 4 °C. Secondary antibodies were used for one-day incubations at 4 °C, after extensive washing of tissue sections. After final washing, we mounted sections on glass slides with anti-bleach preservative medium in sequential order along the rostro-caudal axis. Primary antibodies used in this study were: chicken anti-GFP (Invitrogen, 1:2,000), chicken anti-MYC (Invitrogen, 1:5,000), goat anti-ChAT (Millipore, 1:500), mouse anti-MYC (ATCC, 1:100), mouse anti-V5 (Invitrogen, 1:1,000) and rabbit anti-RFP (Rockland, 1:5,000). Secondary antibodies used were: Alexa Fluor 488 donkey anti-chicken IgY (Jackson, 1:1,000), Cy3 donkey anti-mouse IgG (Jackson, 1:1,000), Cy3 donkey anti-rabbit IgG (Jackson, 1:1,000), Alexa Fluor 488 donkey anti-goat (Jackson, 1:1,000), Cy3 donkey anti-goat IgG (Jackson, 1:1,000) and Alexa Fluor 647 donkey anti-goat IgG (Jackson, 1:1,000). To acquire low-resolution overview images, we used an Axioscan light microscope (Zeiss, 5× objective) and for higher-resolution imaging, we used a FV1000 confocal microscope (Olympus) or a custom-made spinning disc microscope (Visitron).

Anatomical reconstructions

Three-dimensional reconstructions of rostral medulla neurons stratified by projection target. To assess the spatial location, quantitative contributions and overlap between populations of rostral medulla neurons projecting to the contralateral latRM, ipsilateral MdV, ipsilateral MdD and spinal cord, 80-µm-thick coronal brainstem sections were acquired with the 20× objective of

a FV1000 confocal microscope (Olympus), tiling mosaics of multiple fields of view (tile number was variable depending on section size at different rostro-caudal levels) to cover the full section (z-steps of 4 µm). Subsequent stitching and maximum intensity projection images were used as previously described[4,21]. Manual alignment using Amira (Thermo Fisher Scientific) preceded automatic cell-body position assignment with customized image analysis workflows in Knime. Respective regions were assigned using the mouse brain atlas as previously described[29], and as described in 'Virus production, injections and implantations'. Two-dimensional density plots were generated using 2D kernel density estimates, plotting 6 density lines covering the space of 20–100% of highest density equally using the MATLAB function kde2d[54].

Reconstructions of synaptic output of excitatory latRM neurons. To assess major output projections of excitatory latRM neurons, 80-µm-thick coronal brainstem sections or transverse spinal cord sections were acquired with a 40× objective of a confocal microscope (FV 1000, Olympus) or a custom-made spinning disc microscope (Visitron), tiling mosaics of multiple fields of view (z-steps of 2 µm). Subsequent stitching and maximum intensity projection images were generated using custom-made macros in Fiji. Automatic synaptic spot detection was carried out in Imaris (v.9.1.2. Oxford Instruments, Bitplane) and 2D density plots were generated using 2D kernel density estimates, plotting 6 density lines covering the space of 10–100% of highest density equally using the MATLAB function kde2d54. To assess the decrease of synapses derived from excitatory latRM neurons along the rostro-caudal axis in the spinal cord, the total number of detected synapses at C1 was used as a reference to calculate the decrease in synaptic numbers at C5 and C8 levels.

Behavioural experiments

Open field assay. Mice were placed in a 35 × 35-cm square arena, which they were allowed to explore freely for at least 10 min. For single-unit recording experiments, mice were exposed to tasks in a sequential manner, including the open field assay at the end. For loss-of-function and

photometry experiments, open field sessions were carried out after the experimental days during which the pellet task was completed.

Lever task. Mice were kept under water restriction and body weight was monitored to not drop below 85% of the original weight. We used a custom-made behavioural chamber allowing for high-speed videography from the two sides of an ultra-sensitive lever (2g sensitivity, MedAssociates) adapted from previous work[31]. Water rewards (50 µl) were delivered in the chamber at a spatially separate location from the lever in response to single lever presses using electrically controllable water pumps (MedAssociates). Training consisted of exposure to the behavioural box during 3 training days for a maximum of 60 min or 5 (day 1), 10 (day 2) or 20 (day 3) rewards. Experiments with mice that did not achieve at least 20 rewards on the 4th training day were not continued. Selected mice were then trained to reliably achieve at least 20 rewards by pressing the lever during at least 4 more training sessions. The entire training did not exceed two weeks. For analysis, only first-attempt forelimb lever presses (as described in 'Behavioural analysis, scripts and statistics') were used. During experimental sessions, mice were allowed to press the lever for as long as they were engaged in the task to achieve a maximum number of successful trials for analysis. The protocol was applied in closed-loop using an Arduino Uno board (Arduino) coupled with transistor–transistor logic (TTL) pulses recording lever-press time points and triggering water rewards via the Arduino MATLAB extension package (The Mathworks). A synchronizing start TTL pulse was sent from the Arduino Uno board to the OmniPlex recording system to allow for correct alignment of behavioural with electrophysiological data.

Pellet task. Mice were kept under food restriction and body weight was monitored to not drop below 85% of the original weight. A custom-made chamber was designed as previously reported21,30, containing a slit through which mice were trained to reach for a food reward. Movies were taken using one camera from the front and one from the side (Pike, Allied Vision, 200 frames per second (fps)) or only a side camera for photometry experiments (Plexon, 60 fps).

On the first day, mice were allowed to also obtain food pellets with their tongue. On following days, food pellets were placed at a marked, consistent position outside the slit further away, to not allow for tongue retrievals to enforce forelimb reaching trials. The position of the pellet was slightly moved to the side relative to the slit, depending on whether mice were right- or left-handed. Mice were trained for at least 8 days, aiming for a success rate of over 30% and with a goal of retrieving more than 15 pellets or 35 reaches. For loss-of-function experiments, mice with a baseline success rate of less than 30% were excluded. Following the baseline session, mice were injected intraperitoneally first with CNO (10 mg per kg body weight in PBS) and then with PBS, spaced by at least 24 h from each other, followed by another analogous exposure paradigm. CNO or PBS injections occurred 40 min before initiation of the pellet task. For single-unit recordings, mice were exposed to other behavioural tasks consecutively and no success-rate exclusion rate was applied. For photometry experiments, mice were exposed to the pellet task and subsequent food handling. For analysis, only successful, first-attempt forelimb reaches (as described in 'Behavioural analysis, scripts and statistics') were used. For the two-choice pellet reaching task and recordings along the dorsoventral axis, mice were first trained the same way for three sessions with only one slightly shifted pellet position. From the fourth training session onward, a second pellet was placed exactly in the middle at the same distance, aligned with the slit. Mice were trained to reach for both positions to retrieve pellets for at least another 12 sessions before silicon probe implantation. During experimental sessions, mice were allowed to reach for as long as they were engaged in the task to achieve a maximum number of successful trials for analysis. For analysis along the dorsoventral axis, medial and lateral reaches were pooled into one reaching category (as described in 'Electrophysiology analysis').

Handling task. Mice were kept under food restriction as described in 'Pellet task'. During habituation, they were provided with short spaghetti sticks in the home cage and exposed to the testing chamber (10 min, once a day for 2 days). For loss-of-function experiments, the testing

chamber was a 8.2 by 7.1-cm custom-made plexiglass box with transparent floor, mounted on a holder containing a 45°-inclined mirror, allowing for a bottom view of the paws during pasta handling. Movies were taken using one camera from the front and one directed at the mirror (Pike, Allied Vision, 200 fps). During behavioural testing (20-min session), spaghetti sticks (about 2 cm in length) were presented, upon which mice started bilateral handling as previously reported[34]. For data analysis of electrophysiological data, additionally, successful trials in the pellet task resulted in the retrieval of food pellets, thereafter handled with both hands, resulting in qualitatively similar movements as during spaghetti handling. These trials were pooled for analysis.

Grip strength analysis. Forelimb grip strength of mice was tested as previously described[21].

Optogenetic activation experiments. Optogenetic activation of rostral medulla neurons was performed using a PlexBright Optogenetic Stimulation System (Plexon) in combination with laser stimulation (Cobolt 06-MLD; 473 nm; 100 mW). The laser was triggered manually when mice were at rest. Unless otherwise specified, we used continuous light exposure at intensities of 5 or 10 mW. We measured the laser intensity at the beginning of every experimental session at the tip of an optic fibre of the same length as the one implanted to ensure precise and reliable stimulation strength with an optical power meter (Thorlabs). Mouse behaviours and responses were monitored simultaneously with two cameras (Pike, Allied Vision) at 200 fps or a Sony alpha 7s camera (Sony) at 100 fps in an open field environment. For trajectory reconstructions with DeepLabCut55,56 (as described in 'Behavioural analysis, scripts and statistics') high-frame rate videos (uEyeCP, IDS, 450–668 fps) were acquired to allow for successful tracking.

Behavioural analysis, scripts and statistics

Open field assay. To quantify basic locomotor parameters in the open field, videos acquired from above (Pike, Allied Vision, 200 fps or an integrated camera for photometry, 60 fps, Plexon) were used. Mice were placed in a square arena (35 × 35 cm) within a noise-isolated chamber for 10

min. Centre-of-mass body tracking was performed using the CinePlexStudio tracking function (CinePlexStudio v.3.7.1. Plexon) and speed values were calculated from extracted coordinates on a frame-by-frame basis. Whole-body and speed traces were clustered into defined locomotor bouts (>5 cm s−1 for >200 ms) and for analysis of loss-of-function experiments, maximum speed (highest single speed value during a locomotor bout), bout duration and bout distance parameters were calculated using custom-written MATLAB scripts. For electrophysiological recording and photometry experiments, locomotor bout start- and end-points were extracted and aligned with single-unit activity data, as detailed in 'Electrophysiology analysis'. To determine the timing of locomotion swing phase, we annotated ipsilateral forelimb footfalls during open field locomotion, and used the time window 0.1 s before footfall for analysis. Because forelimbs were often not discernable on the recorded top-camera videos, we also used coincidence of diagonal hindlimb footfall data for annotation of forelimb data, a behavioural feature confirmed by video analysis using top and bottom cameras in another dataset.

Lever task. Lever reaching behaviour was recorded using high-speed videography from both sides of the lever (Pike, Allied Vision, 200 fps). Video capture was triggered synchronized with electrophysiology measurements using commercially available software (Omniplex, Plexon). Relevant behavioural time points were extracted manually using CinePlexEditor (v.3.6.0, Plexon). Definition of the behavioural time points was as follows. Time points when the mouse was present and attending in front of the lever were defined as arrival. The video frame in which the forepaw was first observed to lift off the ground or start to move towards the lever from an already slightly lifted position was defined as reaching start. For lever on and off, the first frame in which the paw touched the lever was defined as the onset of the lever phase and the last frame in which the paw was still observed on the lever was defined as the offset. After retrieving the paw from the lever, the last video frame in which the paw was observed in a retraction movement before being placed on the ground or slightly stopped above in the air was defined as the end of retraction. For

electrophysiological analysis, only first-attempt lever-pressing sequences were analysed. Secondary lever-pressing sequences (that is, the immediate initiation of another lever- pressing sequence after the first attempt) were not used for electrophysiological analysis to ensure minimal trial-to-trial variability. These extracted time points were then used for analysis and alignment with electrophysiology data as detailed in 'Electrophysiology analysis'.

Pellet task. Movies taken from the front and side (Pike, Allied Vision, 200 fps) were used for manual assignment of behavioural time points and for coordinate extraction using CinePlexEditor (v.3.6.0, Plexon) or MATLAB (The Mathworks). Synchronization of movies with electrophysiological and fibre photometry data was achieved using commercially available software (Omniplex, Plexon). Movies for photometry experiments were acquired using a system-integrated camera from the side (Plexon) acquiring at 60 fps allowing for precise alignment with calcium transients. For loss-of-function experiments assessing reaching behaviour, success rate was defined as the fraction of successful trials of all reaching attempts when a pellet was presented. Single reaching attempts were defined as whenever the tip of the fingers exited and re-entered the slit opening of the pellet reaching box. Successful trials were defined as the complete successful behavioural sequence composed of reaching for, grasping and retrieving a pellet to the inside of the pellet reaching box. We defined 'miss trials' as trials during which the mouse missed touching the pellet during reaching. To assess directionality defects, the spatial location of the hand at the most extended time point was registered in camera pixel coordinates from both the side and front camera and used for plotting and quantification of the endpoint variability and distance from the pellet using MATLAB. Pixel coordinates were first normalized to a defined spatial constant at the behavioural box and then to the pellet position itself to correct for any potential trial-to-trial effects in pellet or camera positioning. Variability was defined as the area of the ellipse with x and y diameters defined as the average s.d. of all endpoint coordinates in the x and y direction in pixels, respectively. Distance was defined as the average pixel distance of all

the endpoints from the pellet position. For single-unit electrophysiology, behavioural time points were defined as follows. The video frame in which the forepaw was first observed to lift off the ground or start to move towards the slit from an already slightly lifted position was defined as reaching start. Time points at which the fingers started to spread in anticipation of grasping for the pellet were defined as the onset of the grasping movement. Time points during which the pellet was firmly grasped and the retraction sequence initiated were defined as the endpoints of grasping. This often, but not always, coincided with paw supination. After grasping the pellet, the hand is transported towards the mouth; time points at which the pellet arrived at the mouth were defined as retraction endpoints. For electrophysiological and fibre photometry analysis, only first-attempt successful reaching sequences were analysed. Unsuccessful or secondary successful reaching sequences (that is, the immediate initiation of another reaching sequence after an unsuccessful attempt) were not used for electrophysiological and fibre photometry analysis to ensure minimal trial-to-trial variability. Sessions during which mice achieved fewer than four successful reaching sequences were excluded. Further analysis was conducted as detailed in 'Electrophysiology analysis' and 'Photometry analysis'.

Handling task. Handling episodes were recorded using high-speed videography (for electrophysiology, Pike, Allied Vision, 200 fps; for photometry, integrated camera, 60 fps, Plexon) and behavioural time points were defined using CinePlexEditor (v.3.6.0, Plexon) or MATLAB (The Mathworks) as follows. Handling start was defined as the time point at which both forelimbs arrived at the mouth before stereotypic, coordinated handling was initiated. The end of the handling was defined as the video frame in which both forelimbs were retrieved from the mouth and any subsequent food handling ceased. Synchronization with electrophysiological and photometry data was achieved through commercially available software (Omniplex, for electrophysiology, CineLyzer for photometry, Plexon) and analysed as detailed in 'Electrophysiology analysis'. For loss-of-function experiments, handling sessions were recorded

using high-speed videography (Pike, Allied Vision, 200 fps). On the basis of previously reported data34, the following parameters were quantified: number of pasta drops, percentage of time during which the preferred paw is used as guide paw, as well as probability distribution of pasta handling angle. Pasta drop rates were quantified manually, whereas all other quantifications were based on pose estimation performed with DeepLabCut55,56 (as described in 'Optogenetic activation experiments'). The network was trained using at least 200 frames annotated on the following body parts: nose, forepaws and feet, as well as on the extremities and marks on the pasta pellet. Pasta drops were defined as events in which a mouse inadvertently released the pasta pellet from its forepaws, causing it to fall on the floor of the test chamber. For quantification of preferred paw use as guide paw, the guide paw was defined as the one kept closer to the snout during handling (Fig. 2e). For each mouse, the preferred paw was defined as the one preferentially used as a guide paw during the control handling session. After pose estimation, the distance between each paw and the nose was computed over all handling episodes and the time at which 'preferred-hand to nose' distance was shorter than 'non-preferred-hand to nose' distance was calculated as a percentage of the total handling time. For the probability of distribution of pasta handling angle, for each handling frame we quantified the angle comprised between the line fitting the tracked marks on the pasta pellet and the body midline. The body midline was calculated as the line connecting the nose and the midpoint between the feet (Extended Data Fig. 4a). Probability was calculated on the basis of the total number of handling frames, and relative handling angle values were offset from median angle value for each mouse during control sessions.

Optogenetic activation experiments. For analysis of optogenetically induced behaviours, quantification of the reliability to elicit the assessed behaviour upon stimulation was performed manually, using high-speed videography (Pike, Allied Vision, 200 fps, Sony alpha 7s, Sony, 100 fps or uEyeCP, IDS, 450–668 fps). For each mouse, a minimum of 30 optogenetic stimulation

events were scored. Each stimulation event was analysed frame by frame and, whenever laser-induced movements were detected, assigned to the appropriate behavioural category. Reliability percentages for each behavioural category were calculated as the fraction of trials eliciting that specific behaviour from all scored stimulation trials. Behavioural categories referred to in Fig. 4 were defined according to the following observed phenotypes. Reaching was defined as single event, unilateral lifting and extension of the forelimb accompanied only by spreading of individual fingers. Grasping was defined as unilateral lifting and extension of the forelimb in combination with flexing finger dynamics. Tapping was defined as repeated, unilateral lifting of the forepaw without flexing finger dynamics. Hand-to-mouth movement was defined as repeated, unilateral extensions of the forelimb with flexing finger dynamics directed towards the mouth. Grooming was defined as repeated, bilaterally coordinated lifting of the forelimbs and rhythmic swiping over facial areas. Locomotion was defined as coordinated full-body movement involving the repetitive use of all four limbs to translocate the entire body in a coordinated manner. Head turning was defined as horizontal head rotation that did not involve forelimb movements. No behaviour was used for events during which no discernible movement was elicited upon optogenetic stimulation. For analysis of forelimb trajectories during the various different forelimb behaviours elicited from the distinct subpopulations, the machine learning algorithm DeepLabCut55,56 was used in combination with high-speed videography to characterize behavioural phenotypes (uEyeCP, IDS, 450–668 fps). We trained the network with an initial dataset for each kind of elicited behaviour using at least 200 frames to annotate individual parts of the forelimb. Subsequent unsupervised training involved at least 600,000 iteration rounds, after which no improvement of the pose estimation reliability could be observed. Extracted pixel coordinates were plotted using customized MATLAB or Python scripts. For reaching analysis, trajectory coordinates were relative to the resting position of the paw before stimulation. Time coordinates were normalized using the time from movement onset to maximum extension (along the anterior–posterior axis) of the reach episode and discretized into equal bins. For tapping analysis, dorsoventral coordinates were

relative to the resting position of the paw before stimulation. Time coordinates were normalized by the time between motion onset and the maximum dorsoventral position of the tap episode, discretized into equal bins and offset such that t = 0 occurs at the tapping peak. For grooming analysis, trajectory coordinates were relative to the resting position of the paws before stimulation. Time coordinates were normalized by the time between motion onset and completion of a grooming bout, and discretized into equal bins. For EMG experiments, only reaching start time points with respect to the laser stimulation were assessed, aligned to the EMG traces and analysed as detailed in 'EMG analysis'.

Electrophysiology analysis. All spiking time points of single-unit data were imported for further analysis to MATLAB from NeuroExplorer v.5 (Plexon). We determined the distribution of average firing rates for latRM neurons during behaviour and found that most exhibited values below 20 Hz, with only a minority displaying higher values (Extended Data Fig. 1c). To determine how individual neurons contribute to changes in activity profiles, we aligned the relative mean-subtracted firing rates according to timing of peak changes. Spiking events were aligned with individual behavioural time points in a window of ±8 s and for individual behavioural sessions, average firing frequencies were calculated using 50-ms binning. Baseline firing rates were determined during the time window between −6 to −2 s for each behaviour and are indicated separately in displayed raster plots throughout the presented figures (scale of 0–100 Hz). For analysis defining neuronal tuning to task, we used the reaching start as an alignment point in the pellet and lever task, and the start of locomotion in the open field task for locomotion. To illustrate single example neurons graphically, alignment was sometimes performed to different time points as indicated and the display of single trial raster plots was limited to a subset of ten randomly selected trials. For tuning analysis to pellet or lever tasks, we included neurons for which the average firing rate reached 20 Hz at least once during the task-relevant time window (±2.5 s; task-relevant neurons, n = 84 for pellet task, n = 81 for lever task; n = 48 for locomotion). Task-tuned

neurons were selected on the basis of changes in firing rate more than 3 s.d. above baseline firing at least for one bin during the time window of −1.5 s to +0.5 s from onset of the task (n = 49 for pellet task; n = 43 for lever task; n = 4 for open field) (Extended Data Fig. 1). Average overall firing rates of neurons displayed in Extended Data Fig. 1 were calculated from the ±8-s time period for the lever or pellet task individually. To assess task specificity to forelimb behaviours at the population level, we compared the baseline-subtracted firing rate of task-tuned neurons in the pellet or lever task to the activity of the same neurons during open field locomotion or shuffled data (100×) in 250-ms bins (Fig. 1a) (statistical details are provided in 'Statistics'). Heat map plots (Figs. 1b, 3d, Extended Data Fig. 2) were generated from mean-subtracted firing rates normalized for every neuron. Fifty-ms bins were assigned a colour in a 64-colour range, over which the mean-subtracted firings rates were scaled. Baseline firing rates were calculated as average firing rates of individual neurons during the baseline period. The colour scale for the baseline shown in the sidebar was generated by scaling the range of baseline firing rate values over a 64-colour range displaying the 0–100 Hz range. Average firing rates during behaviour were calculated as average firing rates of individual neurons during the behaviour period. Relative behaviour firing rates were calculated as the difference between baseline and average behaviour firing rates (Extended Data Fig. 1d). To determine behavioural-phase tuning correlations, we selected neurons tuned to the behavioural phase of pellet reaching, lever reaching, handling or swing phase of locomotion. We determined the peak firing rate of individual neurons during the respective behavioural phases as defined below (each annotated on a trial-by-trial basis), from which the mean baseline firing rate was subtracted (50-ms bins). Only trials with firing rate changes at least three s.d. above baseline firing frequency, in the annotated time windows for the specific behavioural phase, were included in our analysis. We applied a reliability cut-off of 0.4 for neurons to be included into a behaviourally tuned group. Reliability of a neuronal response was calculated from the number of trials for which the firing rate of the analysed neuron crossed the three s.d. threshold, divided by the total number of trials recorded. Additionally, to be included in the behaviourally tuned group, a neuron must

have reached an average firing rate of at least 10 Hz during the task time window, and a maximum average firing rate that is greater during the behavioural phase than the baseline. The time window used for analysis of pellet or lever reaching was confined to 1.5 s before reaching onset to the end of the reaching phase. For handling, the time window used for analysis was from the start of handling onset to the end of handling. Determined maximum trial-averaged firing rate values in the defined behavioural phase of the analysed neurons subtracted by the maximum trial-averaged baseline firing rates were plotted against each other and correlated to assess significance (Extended Data Fig. 2e) (as discussed in 'Statistics'). For visualization purposes, 5 data points above 30 Hz and 2 below −5 Hz contributing to the regression line are not displayed in top left panel of Extended Data Fig. 2e. For recordings along the dorsoventral axis of latRM, we plotted the average baseline-subtracted peak firing rate of significantly behaviour-tuned neurons in the two dorsal recording depths (Fig. 3c top; aligned to handling onset) and two ventral recording depths (Fig. 3c bottom; aligned to reaching onset). The activity of the reaching- and handling-tuned neurons in these recordings was compared to the activity of the same neurons shuffled randomly (100×) in 250-ms bins (Extended Data Fig. 7b) (statistical details are provided in 'Statistics'). The four recorded depths are marked by colour bars next to raster plots of individual neurons, with two shades of magenta indicating dorsal depths and two shades of cyan indicating ventral depths. For directionality analysis, task-tuned neurons in either direction were selected and relative average peak behaviour firing rates (average peak behaviour firing rate – average baseline firing rate) were calculated for both directions separately. The directionality index is the difference in average peak firing rates for the two directions in Hz. For plotting, we sorted the differential firing rates in ascending direction. We included a shadow depicting the standard deviations during the baseline of both directions for the corresponding neuron in the plot (Extended Data Fig. 3).

EMG analysis. For analysis of latencies and plotting of the EMG data (Extended Data Fig. 10) amplified and bandpass-filtered raw signals were used for further analysis. A baseline period of 200 ms before the reaching start (as described in 'Pellet task' in 'Behavioural analysis, scripts and statistics') or the laser onset was used to calculate the average baseline activity and s.d. After mean subtraction, a threshold of three s.d. of the baseline was used to derive latencies for the different muscles when the raw trace crossed this threshold for at least four consecutive frames. We analysed at least ten trials per mouse and condition. For the relative onset of muscle activity, average activation time points were normalized to time between the reaching start and the point of maximum forelimb extension (as described in 'Pellet task' in 'Behavioural analysis, scripts and statistics'). For the average plot, the raw trace was smoothened using a moving average window (29 frames for laser and 99 frames for pellet reaching).

Photometry analysis. Raw fluorescence and background fluorescent data were used to calculate ΔF/F values based on a 3-s moving-average window. Recording sessions in which the mean value of the 1,000 maximum ΔF/F single-frame peaks was either 50% higher or lower than on the first day of recording were excluded. Fluorescent traces were then aligned with individual behavioural events (reaching, handling or locomotion start) and normalized in between the maximum and minimum ΔF/F values observed during all recording sessions. For shuffled data, the same number of random time points as pellet-reaching events was generated from the pellet-reaching experimental session. Average traces were plotted on a time scale from −1 to 5 s around the respective behaviour.

Plotting and programs. All plots, scripts and analysis were generated or performed in MATLAB v.2017b (The Mathworks), Python3 (www. Python.org) or GraphPadPrism7 (GraphPad) and figures were assembled using CorelDRAW X6 to X9 (Corel). Mouse drawings were provided by E. Tyler and L. Kravitz through the SciDraw repository (www.scidraw. io) and adapted in Corel X6 or X8.

Statistics. Significance levels indicated are as follows: *P < 0.05, *P <0.01, ***P<0.001, unless otherwise specified. All data are presented as mean ± s.e.m., except where otherwise indicated. In all statistical comparisons, normality of the data was checked with quantile plots and/or with D'Agostino and Pearson, Shapiro–Wilk and Kolmogorov– Smirnov normality test in Prism. Non-normally distributed data were subsequently compared with non-parametric tests. The following statistical tests were used to assess significance when indicated. Firing specificity of latRM neurons according to task (Fig. 1a) was assessed by comparing the peak firing rates of 250-ms bins in the task window (defined by −1.5 to 0.5 s) between all neuronal data pairwise with the Wilcoxon signed-rank test. The Bonferroni correction was applied to account for multiple comparisons and the significance levels were adjusted as *P < 0.0167, **P < 0.00033, ***P < 0.00033. For shuffled data, the average P value of all shuffles (100×) was used to assess significance (P values: pellet task versus shuffled: <0.0001; pellet task versus locomotion: <0.0001; locomotion versus shuffled: 0.245; lever task versus shuffled: <0.0001; lever task versus locomotion: <0.0001; locomotion versus shuffled: 0.568). Similarly, the activity of neurons along the dorsoventral axis, specifically tuned to the behavioural time window of reaching or handling, was compared to the shuffled data (Extended Data Fig. 7b: pellet reach versus shuffled: P ≤ 0.0001; handling versus shuffled: P ≤ 0.0001). The same approach was used to probe the activity of the handling-tuned and lever-reach-tuned latRM neurons during other behaviours, with a Bonferroni correction for 4 comparisons leading to adjusted significance levels of *P< 0.0125, **P < 0.0025, ***P < 0.00025 (Extended Data Fig. 2a, b; time window was defined from 0 to 2 s only for pellet-reaching aligned activity for the handling-tuned neurons as the onset of activity was delayed with respect to reaching start; P values in Extended Data Fig. 2a: pellet reaching versus shuffled: P ≤ 0.0001; handling versus shuffled: P ≤ 0.0001; lever reach versus shuffled: P = 0.2281; locomotion versus shuffled: P = 0.9523; in Extended Data Fig. 2b: pellet reaching versus shuffled: P = 0.002548; handling versus shuffled: P = 0.201408; lever reach versus shuffled: P ≤ 0.0001; locomotion versus shuffled: P = 0.700481). To quantify action cotuning

between different behaviours (Extended Data Fig. 1d) we used a Spearman's rank correlation test to assess significance (Spearman r and P values, upper left r: 0.43539, P: 0.00673; lower left r: −0.39194, P: 0.01495; upper right r: 0.39915, P: 0.02888; lower right r: -0.1315, P: 0.48852). All data shown in Fig. 2 and Extended Data Fig. 3 were compared using the two-sided paired t-test unless otherwise specified (P values in Fig. 2b left experimental: <0.0001; Fig. 2b left control: 0.3539; Fig. 2b right, from left to right: <0.0001, 0.0003, <0.0001, <0.0001; all other comparisons within CNO or within the PBS group did not result in significant changes; Fig. 2c: 0.0002; a Wilcoxon signed-rank test was used for Fig. 2f: 0.007 and Fig. 2g: 0.006; Extended Data Fig. 3b left: 0.5601; Extended Data Fig. 3b middle: 0.6002; Extended Data Fig. 3b right: 0.3892; Extended Data Fig. 3c left: 0.0029; Extended Data Fig. 3c middle: 0.0073; Extended Data Fig. 3c right: 0.0034; Extended Data Fig. 3e left: 0.0162; Extended Data Fig. 3e middle: 0.0148; Extended Data Fig. 3e right: 0.0095). Grip test analysis in Extended Data Fig. 4b is shown as percentage on the PBS day using a Wilcoxon rank-sum test (0.4237). Overlap ratios between distinct latRM or medRM subpopulations in triple injections are displayed as averages of all mice with respective subpopulation as a reference (Extended Data Fig. 6b; latRM, left: 19.2 ± 5.5% and 17.2 ± 5.1%, middle: 12.3 ± 3.1% and 6.9 ± 1.4%, right: 7.3 ± 0.6% and 4.1 ± 1.3%; Extended Data Fig. 6c; medRM: 70.9 ± 18.7% and 53.8 ± 13.2%). To compare spatial distributions of latRM subpopulations between the medRM and latRM (Extended Data Fig. 6c), we used a two-sided paired t-test (P values: spinally projecting: 0.0019; MdV-projecting: 0.0037; contralateral-projecting: 0.0058; MdD-projecting population: 0.0162). Reaching trajectory endpoints (Extended Data Fig. 9b, right) were compared using the summed distance of individual endpoints to the centroid (grouped by mouse, distance = 718 pixels; all mice grouped together, distance = 1,025 pixels). A two-sided, unpaired t-test was used to compare EMG responses after light stimulation (Extended Data Fig. 10b; P values: latency biceps versus triceps: 0.0093; relative onset for biceps versus triceps: 0.0383).

Acknowledgements We thank M. Sigrist, M. Mielich, P. Marini, M. Cases Escuté, P. Capelli and K. Fidelin for experimental help; K. Yamauchi for help with computational analysis of behaviour; L. Gelman and J. Eglinger from the FMI imaging facility and N. Ehrenfeuchter from the Biozentrum imaging facility for help and advice with image acquisition and analysis; J. Courtin (FMI) and members of the Moser laboratories (Trondheim) for advice and help with the acquisition and analysis of the single-unit recordings; P. Argast and P. Buchmann from the FMI mechanical workshop for building devices for behavioural experiments; M. Stadler for help with statistical analysis; and P. Caroni for discussions and comments on the manuscript. All authors were supported by funding from the European Research Council (ERC) under the European Union's Horizon 2020 research and innovation programme (Descent, grant agreement no. 692617), the Swiss National Science Foundation, the Kanton Basel-Stadt and the Novartis Research Foundation.

Author contributions All authors were involved in the design of experiments. L.R. together with C.P. carried out most experiments, and acquired and analysed data. R.S. was mainly involved in functional and anatomical experiments related to intra-brainstem interactions, fibre photometry experiments and loss-of-function experiments. H.K. was involved in electrophysiology analysis and loss-of-function experiments. S.V.-G. was involved in early experiments related to intra-brainstem interactions and anatomy. S.A. initiated the project, designed experiments, analysed data and wrote the manuscript. All authors discussed the experiments and commented on the manuscript.